Structural Investigation of Zungeru-Kalangai Fault Zone, Nigeria using Aeromagnetic and Remote Sensing Data

Augustine Babatunde Arogundade[1,1], Musa Olufemi Awoyemi[1,1], Olaide Sakiru Hammed[2,2], Sesan Cornelius Falade[3,3], and Ojudoo Darius Ajama[1,1]

[1]Obafemi Awolowo University
[2]Federal university Oye-Ekiti
[3]Landmark University Omu-Aran

November 30, 2022

Abstract

The aeromagnetic and satellite imagery data of the part of northcentral Nigeria were processed to delineate subsurface structures, produced 2D models of the structures within the study area with a view to establishing the existence of the Zungeru-Kalangai fault zone geophysically. The lineaments extracted from the Landsat-7 ETM+ imagery are dense around Zungeru, Tegina and Gidan Karauku area in the southwestern part of the study area, in the southeastern parts particularly around Chikun area and also in the northern part around Kwaimbana and Doka. The N-S, NNE-SSW and NE-SW lineament trends are prominent on the Landsat-7 ETM+. The inferred faults delineated from the aeromagnetic data showed that striking NE-SW trend is predominant. The derived composite map of the inferred faults extracted from aeromagnetic data and the surface lineaments delineated from the satellite imagery superimposed on the existing faults revealed the presence of several undetected faults cutting across the study area. The location and orientation of the Zungeru/Kalangai fault zone in the northcentral part of Nigeria which extend about 245 km, correlate with the existing fault on the published geological map of Nigeria and showed that it possibly projected to the study area through the basement within Bida Basin from the southwestern part of Nigeria. The results of the 2D models confirmed the existence of the Zungeru-Kalangai fault zone and other several new faults such as faults f3 (northern part), f4 (located around Kaya in the northeastern part of the study area), f6 and f9 (located around Sengiakun area in the northwestern part of the study area) with their approximate source locations and dips. Conclusively, these study confirm geophysically the existence of the Zungeru-Kalangai fault zone which is dipping NW and other unmapped major structures in the study area.

Structural Investigation of Zungeru-Kalangai Fault Zone, Nigeria using Aeromagnetic and Remote Sensing Data

A. B. Arogundade[1], M. O. Awoyemi[1], O. S. Hammed[2], S. C. Falade[3], O. D. Ajama[1,4].

[1]Obafemi Awolowo University, Il-Ife, Nigeria

[2]Federal university Oye-Ekiti,

[3]Landmark University Omu-Aran, Kwara State

[4]Ondo State Ministry of Education, Science and Technology

Corresponding Author: Augustine B. Arogundade (arogundadeab@oauife.edu.ng)

Key points

- The location and orientation of the Zungeru/Kalangai fault zone possibly projected to the study area through the basement within Bida Basin.
- The presence of several major faults with and without surface expression corresponding to some unknown and known faults were revealed.

Abstract

The aeromagnetic and satellite imagery data of part of northcentral Nigeria were processed to delineate subsurface structures, produced 2D models of the structures within the study area with a view to establishing the existence of the Zungeru-Kalangai fault zone. The lineaments extracted from the Landsat-7 ETM+ imagery are dense around Zungeru, Tegina and Gidan Karauku area in the southwestern part of the study area, in the southeastern part particularly around Chikun area and also around Kwaimbana and Doka (northern part). The N-S, NNE-SSW and NE-SW lineament trends are prominent on the Landsat-7 ETM+. The faults delineated from the aeromagnetic data showed that NE-SW trend is predominant. The derived composite map of the faults extracted from aeromagnetic data and the surface lineaments delineated from the satellite imagery superimposed on the existing faults revealed the presence of several undetected faults across the study area. The location and orientation of the Zungeru/Kalangai fault zone in the northcentral part of Nigeria which extend about 245 km, correlate with the existing fault on the published geological map and showed it possibly projected to the study area through the basement within Bida Basin. The results of the 2D models confirmed the existence of the Zungeru-Kalangai fault zone and other several new faults such as faults *f3* (northern part), *f4* (northeastern), *f6* and *f9* (northwestern) with their approximate source locations and dips. Conclusively, these study confirm geophysically the existence of the Zungeru-Kalangai fault zone which is dipping NW and other unmapped major structures in the study area.

Plain Language Summary

The study establish the Zungeru-Kalangai fault zone geophysically and the essential role of the fault zone on the faulting system of the area. The presence of several unknown major faults with and without surface expression were revealed with the combined interpretation of satellite imageries and high resolution aeromagnetic data. The results of the 2D models confirmed the existence of the Zungeru-Kalangai fault zone and other several new faults such as faults *f3* (northern part), *f4* (located around Kaya in the northeastern part of the study area), *f6* and *f9* (located around Sengiakun area in the northwestern part of the study area) with their approximate source locations and dips.

Keyword: Modelling, Subsurface Structures, Remote Sensing, Aeromagnetics, Fracture Zones, Source Edge Detection

1. Introduction

The Precambrian Basement Complex of Nigeria as an integral part of the West African Craton is known to have been subjected to various episodes of deformation. Studies have suggested the inland extension of the oceanic fracture zones (Romanche and Chain fracture zones) into the Nigerian Basement Complex (Wright, 1976). The Ifewara and Zungeru-Kalangai fault zones in the western parts of Nigeria, which extends over hundreds of kilometres are assumed to be connected with the Romanche and Chain fracture sets (Wright, 1976; Ajakaiye et al., 1986). Adepelumi et al. (2008) investigated the Ifewara transcurrent fault system using integrated geophysical methods across conspicuous weakness zone noticeable in Landsat MSS and SLAR imageries in the Basement Complex of southwestern Nigeria. Quantitative interpretation of the magnetic data showed a near-vertical fault feature, trending in the NNE–SSW direction. Low resistivity zones observed in the area were suggested to be formed by shearing activities during late Precambrian times. The study confirmed the existence of the Ifewara fault and assisted in having an understanding of the tectonic history of the Ifewara shear zone.

Kolawole and Anifowose (2011) analysed the dextral discontinuity along Ifewara-Zungeru area, Nigeria. Detailed study of the lateral extent of this speculated shear zone utilizing Google Earth imagery and field mapping of some particular areas that have been recognized from the satellite imagery were carried out. Three major lineament trends (0°-10°, 160°-170° and 170°-180° directions) were delineated both from the Google Earth imagery and field observations. The results revealed that a section of the megastructure show a strike-slip (dextral) fault zone with a drag towards the North-North-West direction in Zungeru area and deduced that in order to further examine the impact of this discontinuity on the geodynamic history of the study area there is the need for more structural as well as geophysical investigation around the Zungeru segment of the megastructure, hence this study.

Awoyemi et al. (2017a, 2017b) carried out a geophysical mapping to investigate the possible extension of Ifewara fault zone beyond Ilesa area, southwestern Nigeria to parts of Bida Basin, northcentral Nigeria. Analyses involving horizontal gradient magnitude, analytic signal amplitude and Euler deconvolution were carried out on the aeromagnetic data to delineate the Ifewara fault zones which extends through the Bida Basin. The study revealed that a number of minor and major faults with a dominant NNE–SSW and NE-SW trends associated with the Ifewara fault cut across the study area. The study concluded that there is an evidence of the continuation of Ifewara fault zone through Bida Basin to the northern Nigeria.

A number of investigations have been carried out on the lineament analysis over parts of Nigeria. However, the structural attributes (such as depth, dip and strike) of the fault system have not been fully delineated and studied. Therefore, detailed information on the structural attributes and regional geophysical evidence of the Zungeru-Kalangai fault zone is needed to obtain a structural map of the fault zone and its environs. This will be done by using a combination of High Resolution Aeromagnetic Data (HRAD) and satellite remote sensing technique.

2. Geological Description of the Study Area

The zone enclosed by this study is underlain by three low-grade metamorphic belts of semi-pelitic and pelitic schists (Kushaka and Birnin-Gwari formations) (Obaje, 2009) and are fault-controlled rift-like structures (Olade and Elueze, 1979). These schist belts is enclosed by migmatite-gneiss-quartizite complex in the Kusheriki schist group.The Birnin-Gwari schist formation is flanked with Zungeru Mylonites on both sides and strike the western sideof the Kushaka belts. Ajibade et al. (1979) stated that the contact between the Zungeru mylonite identified within some schist belts, the basement and between the gneissic complexes are not metamorphic but tectonic. The Zungeru-Birnin Gwari schist belt comprises the underlying quartzo-feldspathic rocks of the Zungeru granulite formation and the Birnin Gwari schist formation. The Zungeru granulite formation outcrops on both side of the schist belt. It is largely made up of fine-medium grained quartzo-feldspathic rocks which are interbedded with amphibolites and some quartzites. The Birnin Gwari schist formation occupies the synclinal axis of the schist belt with the lower part consisting ofhigher grade biotite-muscovite schists in the east and finely banded phyllites in the west. The Kushaka schist belt which is known in the area to host gold mineralization forms a number of curving schist belts, disjointed by anticlines and domes of gneiss. The littler scale structures in Kushaka schist belt as described by Grant (1978) have a more complex and longer history. In contrast, the Kushaka schist belts are invaded extensively by plutons of granodiorite, syenite and granite, which often penetrate the axial zone of the belts. The geological map of the study area is shown in Figure 1.

3. Methodology and Data Processing

3.1 Landsat ETM+ Data Acquisition and Processing

Multispectral Landsat Enhanced Thematic Mapper Plus (Landsat ETM+) imageries among others provide a number of bands in the short wavelength infrared (SWIR), thermal infrared (TIR) and visible regions, concentrated on particular spectral features due to various types of surface. The choice of the satellite imagery used was based on the availability, spatial resolution and acquisition date as well as the user need. The capturing date of the data falls within the dry season in which there is lesser vegetation cover, thus accentuating features with subtle physiographic expression and making the imagery more suitable for studying maximum surface anomalies.

Four Landsat-7 ETM+ scenes (190/53,190/52,189/53.189/52) of February, 2002 were obtained from United States Geological Survey (USGS) and projected to WGS 84 UTM zone 32 N. The bands from the imagery were mosaicked in order to produce a seamless single image from which a subset covering the area of study bounded by Latitudes 9^{o} 30′ N - 11^{o} 30′ N and Longitudes 6^{o} 00′ E - 7^{o} 30′ E was generated and used for this study. Since each band of Landsat ETM+ imagery has different application purposes, the Optimum Index Factor (OIF) developed by Chavez et al. (1982) was used to select the optimal combination of three bands of the Landsat-7 ETM+ satellite imagery.

The higher the value of the three band combination, the wealthier the information content. Bands 3, 5 and 7 were selected for false colour combination (FCC) (Figure 2) as they have the

highest OIF value of 81.47. The 30 m resolution FCC imagery was merged with 15 m high resolution panchromatic data (band 8) in order to enhance the visual quality of imagery. Linear contrast stretching technique was applied to the pan-sharpened FCC image in order to accentuate the contrast of the imagery bymodifying the values in the 0 - 255 grey level range of individual band of the FCC image. Thereafter, the noise present in the contrast stretched image was removed and the edges were enhanced using the median filter edge enhancement technique for lineament extraction.

The automatically extracted lineaments from the Landsat-7 ETM+ imageries in vector format were overlaid on Google Earth satellite image in order to remove false lineaments resulting from anthropogenic features such as roads and lineament errors such as those occurring at the boundary of the subset satellite imagery and too close, or overlapping lineaments (Hung et al., 2005; Mallast et al., 2011).

3.2 Aeromagnetic Data Acquisition and Processing

The High Resolution Aeromagnetic Data (HRAD) used were acquired from the Nigerian Geological Survey Agency (NGSA) on a flight line in the direction NW-SE. They were spaced 500 m apart and the tie lines in the direction NE-SW at a nominal spacing of 2 km. The nominal flight height was 80 m above the terrain. The removal of IGRF was based on epoch date of 1st of January 2005. The HRAD were interpolated into a uniform grid at 100 m spacing using minimum curvature gridding method to produce a Total Magnetic Intensity (TMI) map. The TMI map was reduced to the equator to correct the effect of the magnetic inclination. The field inclination and declination used for Reduction to Equator (RTE) of the study area were -2.28^{o} and -1.78^{o} respectively (World Magnetic Model Epoch, 2005). The RTE removes anomaly asymmetry caused by inclination and locates the anomalies over the causative bodies. Upward continuation to a height of 100 m was applied to the RTE map to improve the signal-to-noise ratio and attenuate the noise/cultural features in the data. Analytic Signal Amplitude (ASA), Total Horizontal derivative (THD) and Euler Deconvolution (ED) methods were applied to the upward continued RTE map to determine the source edges and their possible depths of occurrence. The resulting maps were integrated to produce a magnetic lineament map. Structural map of the study area was generated from the lineament extracted from the Landsat imagery and aeromagnetic data. The RTE map was subsequently used to produce 2D models for the subsurface structures delineated within the study area.

4. Results and Discussion

The extracted lineaments in Figure 3 were the cumulative outcome of the processed Landsat-7 ETM+ imagery. It is apparent from the Landsat-7 ETM+ lineament map (Carved areas; Figure 3) that the lineaments trending in the NE-SW direction are dense around Zungeru, Tegina, Gidan Karauku and Kusheriki area enclosing with mylonites (Kolawole and Anifowose, 2011) in the southwestern part of the study area. It is also apparent that concentration of lineaments is evident in the southeastern parts particularly around Chikun area and in the northern part around Kwaimbana and Doka trending mostly in the NW-SE directions. The areas with

relatively high lineament density are identified as areas of high degree of rock fracturing. The azimuth-frequency diagram derived shows that the study area is traversed by various lineament trends. The N-S, NNE-SSW and NE-SW trends are prominent on the Landsat-7 ETM+ while NNW-SSE, NW-SE, E-W and ENE-WSW trends are less prominent. The ample extent in the azimuths of the lineaments is due to the polycyclic migmatite, gneiss and granite terrain (Turner, 1983) which constitute major lithology of the schist belt in the study area.

The variation in the magnetic field intensity across the TMI map (Figure 4) is ascribed to the differences in magnetic mineral content between different rock units and variation in the depth of the underlying rocks (Figure 4). The magnetic intensity values on the TMI map ranged from -82.1729 to 107.5586 nT. Some of the areas observed with high magnetic intensity value are Jigbeji (lower part of the study area) with anomalies trend in the E-W direction, parts of Sengiakun and Mutumji (Northwest). Areas with minimum magnetic intensity value of -82.2 nT are dominant around Sengiakun. Rocks characterized with low intensity in low latitude area (such as the study area) usually have high susceptibilities while rocks with high magnetic intensity usually have low magnetic susceptibilities. Linear anomalous zones trending in the NE-SW and NW-SE directions are discerned on the TMI map. The NE-SW trending linear anomalous zone extends from Bogi-Zungeru area (Southwest) to Giwa area (northeastern portion of the study area) while an elongated NW-SE trending anomaly was observed in the northeastern part of the study area. A qualitative examination of these conspicuous magnetic patterns revealed that the linear anomalous zones are reflected by magnetic lows bounded by magnetic highs and can be interpreted as reflecting an extensive structure in the Precambrian Basement.

In order to highlight the contact locations and directions, the THD and ASA maxima (that is, the source edge locations) was overlaid on the THD and ASA maps respectively (Figs. 5 and 6). The directions of various forms of linear maximum amplitudes on the THD and ASA maps were also similar. The maximum amplitudes on the THD and ASA correspond to geological contacts.

The result of 3D Euler deconvolution (ED) for the study area is shown in Figure 7. Reid et al. (1990) indicated that a suitable structural index used is reflected with a clustered solutions. Therefore, in order to locate faults and their depths of occurrence within this study area, a structural index of one (1) which depicts a dyke/fault (Reid et al., 1990) was selected for this study and gave a well clustered solutions. The Euler solutions show the spatial locations and non-uniform depths of the interpreted structures (Figure 7). The linear solutions are therefore interpreted as faulted block boundaries. These solutions matched with the source edges that were also delineated with the ASA and THD methods. Non-uniform depths range of 180 to over 900 m were distributed across the study area. Some important zones evident on the Euler plot are made noticeable by oval shapes (L1 to L4). L1, which shows contiguous solutions with non-uniform depths is approximately trending in NE-SW direction outstretching to the northeastern part from the southwestern part (Bogi-Zungeru) of the study area and it served as conjugate pair to L2 solutions. L2 and L3 observed in the northeastern and northwestern part

respectively mark a series of NW-SE trending solutions. Linear solutions enclosed in an oval shape labelled L4, bisected by L3 solutions, is also observed in the northwestern part.

4.1 Composite Map

The composite map of all the source edge detection techniques was produced by superimposing the maxima of ASA (brown), THD (pink) and Euler solutions (black) (Figure 8). The matching maxima/solutions of THD, ASA and ED are indicative of subsurface rock boundaries which could be lithological contacts or structures. Apart from this reliability deduced from the use of more than one technique for locating the magnetic source edges, the conflation of these techniques has diverse implications on the strike, length, dip direction and depth of the subsurface structures.

4.2 Inferred Contact Locations

The contact locations (Figure 9) inferred from THD and ASA trend in various directions, dominantly in N-S, W-E and NE-SW. Other trends observed on the azimuth-frequency diagram are in NNE-SSW, WNW-ESE, NW-SE, NNW-SSE and ENE-WSW directions. Across the study area, some contact lineaments extend several kilometres. These contacts may be a representation of elongated boundaries, ormajor faults between different rock units that might have been affected by the same tectonic history.

4.3 Inferred Faults and Investigation of Zungeru-Kalangai Fault

The inferred faults are composed of major and minor faults or contiguous faults (Figure 10). The inferred lineament map and its associated azimuth-frequency diagram showed that the faults inferred trending in NE-SW, ENE-WSW. E-W and NW-SE directions, among which NE-SW trends are dominant. Other trends identified on the azimuth-frequency diagram are N-S, NNE-SSW and WNW-ESE trending fault systems. Similar trends of structures close to each other are plausible to have resulted from the same tectonic process or processes (Awoyemi et al., 2017a).

Wright (1976) opined that the Chain and Romanche fracture zones of the oceanic fractures could be linked to the prominent NNE-SSW and NE-SW shear zones of the southwestern Nigerian Basement which is in concordance with the major faulting associated with the schist Belt of the northern Nigeria. The pattern of these fracture systems was probably established during the Pan-African Orogeny (McCurry, 1971). Apparently, the NE-SW, ENE-WSW and NW-SE lineament trend identified from Landsat imagery and aeromagnetic map can be taken as significant features of the tectonic framework in the Nigeria Basement Complex (Oluyide, 1988; Olasehinde et al., 1990).

The inferred faults extracted from HRAD and the surface lineaments delineated from the satellite imagery were superimposed on the existing faults shown on published geological map of Nigeria for possible correlation (Figure 11). With the result presented from the composite map, several undetected lineaments traversing the study area were revealed. Some of the interpreted inferred faults corresponds to multiple lineaments at the surface. However, a number of the interpreted fault have no surface expression which suggests they are buried

faults. The surface lineaments are denser on the Landsat ETM+ imagery than on the HRAD due to the fact that the datasets respond to different physical properties of the geological units and features. The difference in the physical properties of the different techniques is due to the fact that aeromagnetic dataset respond to susceptibility contrasts of rocks, while the satellite imagery relies on surface radiation reflectance.

From Figure 11, the location and orientation of the major fault labelled *f2* which extend about 245 km, indicate the Zungeru/Kalangai fault zone in the northern part of Nigeria and show a close spatial correlation with the existing fault on the published geological map of Nigeria. The inferred lineament map shows that the Zungeru/Kalangai fault zone projected to the study area through the basement within Bida Basin from the southwestern part of Nigeria (Awoyemi et al., 2017a, 2017b) and cuts through Bogi, Zungeru passing through Tegina, Kafura Kan Hauwa, Kadaura to Giwa and show continuation beyond the study area. According to Onyedim and Ocan (2001), the Ifewara-Zungeru/Kalangai shear zone probably existed with the emplacement of the mylonites both at Ifewara and Zungeru areas, thus suggesting that the mylonites might have been produced as a result of Pan-African shearing along the Zungeru/Kalangai fault. Many other NE-SW trending faults in the study area could be associated with the stress history of Zungeru/Kalangai fracture system. Close lineaments in the same orientation/direction with the Zungeru/Kalangai fault show they are likely to have the same tectonic origin. The fracturing might have resulted as a response to the regional stress propagating through the study area resulting in approximately NE-SW direction. Also observed on the lineament map is the NE-SW trending Zungeru-Kalangai fault (*f2*) intersected by a NW-SE trending fault (labelled *f4*), creating a conjugate pair around Kaya area in the northeastern part. Also, a NE-SW trending fault *f9* around Sengiakun is bisected by faults *f6* and *f7* in the northwestern part of the study area. The NE-SW trending fault *f9* might have resulted from the stress history of the Zungeru-Kalangai fault zone and is likely to have the same tectonic origin.

5. Magnetic Modelling

In order to confirm the location of the delineated faults, their dips and depth of occurrences in the area, 2D modelling was performed. The 2D forward modelling creates models that represent the basement topography with magnetic properties that gives a magnetic anomaly model similar to the observed field. Ten profiles were taken in directions orthogonal to the prominent inferred faults to confirm their existence (Figure. 12a). The locations of the inferred faults were taken into consideration for the modelling. Euler depth solutions were obtained across each profile and the depth result from Source Parameter Imaging (SPI) technique was used as control across the profile for basement topography (Figure 12b).

Profile A-A' extends a distance of 25.7 km and was taken around Zungeru area, southwestern part of the study area in the NW-SE direction. The observed anomalies along this profile ranged in magnetic intensity from -55.38 to 53.41 nT. The Euler solutions along the profile have a depth range of 245.7 to 743.6 m. The anomaly on Figure 13 showed a magnetic response characterized by a negative low anomaly that occurs between positive high anomalies. For example, the shape of the anomaly shown with oval-shaped (blocks 5 and 9) on Figure 13 is a

typical representation of a thin dyke which shows a relatively high susceptibility (0.003 cgs) than the surrounding blocks (0.002 cgs) while the anomaly marked by a rectangular-shaped (bounding blocks 11, 12 and 13) is a representation of a thick dyke. The model was complemented by Euler depth solutions. The faults *f1*, *f2* and *f8* correspond to those labelled along profile A-A'. Fault *f2* indicate the Zungeru-Kalangai fault zone whose source locations occur at depth range of 266 to 602 m has a magnetic response which depicts a thick dyke. From the model, this anomaly representation confirmed that the Zungeru-Kalangai fault is a fault zone and dipping SE. Also, a minor fault *f1*and *f8* along the profile occur at depth range of 373 to 619 m. According to Gettings (2005), Isaksson et al. (2007), the magnetic susceptibility of rocks reduces as a result of alteration of rock from fractures. Thus, the low susceptibility observed within the area might be as a result of fractured/faulted rock.

Profile B-B' was taken in the NW-SE direction along Kwona Mutua and Kufura Kan Hauwa located at central part of the study area cutting through the central part and lower part of the inferred faults labelled *f2* and *f3* respectively. It extends a distance of 30.9 km and the observed magnetic intensity along the profile ranged from -59.22 to 15.03 nT. This profile (Figure 14) was modelled as sixteen (16) basement blocks whose boundaries are associated with structural features (e.g contacts and faults). The Euler depth solutions across the profile ranged from 198.7 to 1147.6 m. Blocks 6 to 12 are displaced by resulting effect from faults *f2* and *f3* . The magnetic response in carved rectangular-shape between blocks 6 to 12 is characterized by negative low anomalies bounded by positive anomalies which shows a representation of a thick dyke. Fault *f2* is dipping SE and confirms the Zungeru-Kalangai fault zone as also confirmed by profile A-A'. The source locations of fault (*f2*) at this point ranged from 198 to 809 m. Fault *f3* might have been initiated by the tectonic history that affected the Zungeru-Kalangai fault zone.

Profile C-C' was taken along SSW to NNE direction around Dan Dume and Kaya in the northeastern part of the study area. This profile covers a distance of 32.9 km as shown in Figure 15. The intensity of the magnetic anomalies ranged from -25.74 to 25.74 nT. The presence of V-shaped anomalies and the Euler depth solutions above blocks 6 to 10 and block 4 shows it is most likely to be a dyke (thick and thin dyke respectively). Blocks 6 to 10 are displaced by fault *f4* and has a typical magnetic response of a thick dyke. Fault *f4* in the northeastern part of the study area form a conjugate pair with fault *f2* (Zungeru-Kalangai fault zone) as shown in Figs. 11 and 12. The source locations of this fault (*f4*) is complemented by Euler depth solutions which ranged from 218 to 447 m. A minor fault *f5* along profile with depth range from 195 to 467 m occur at block 4 has a magnetic response of thin dyke dipping NNE. The Euler depth solutions across the profile C-C' ranged between 174.4 to 811.4 m.

Profile D-D' covers a distance of 29.9 km and was taken along SW-NE direction passing through parts of Dan Dume and Giwa in the Eastern part of the study area (Figure 16). The intensity of the magnetic anomalies along this profile ranged from –115.54 to 73.57 nT. This area was modelled as ten (10) blocks with susceptibility values ranging from 0.001 to 0.004 cgs. The solutions occurred at depth ranging from 97.3 to 1227.9 m. Blocks 3 (0.003 cgs) and 7 (0.004 cgs) show a magnetic response of a thin dyke with a relative high susceptibility than the surrounding blocks and are displaced by two major faults *f6* and *f7* which are dipping SW

and vertical respectively within the study area. The Euler depth solutions obtained across fault *f6* ranged from 176 to 451 m while that of fault *f7* ranged from 191 to 665 m.

Profile E-E' was taken in the NW-SE direction around Sengiakun in the northwestern part of the study area. This profile (Figure 17) was modelled as eleven (11) basement blocks and extends a distance of 28.5 km. The observed magnetic intensity along the profile ranged from -61.95 to 25.69 nT. The profile was complemented by Euler depth solutions which ranged from 231.23 to 1021.9 m. The magnetic response above block 8 which is displaced by fault *f9* shows a typical representation of a thin dyke with a relatively high susceptibility of 0.002 cgs than the surrounding blocks (0.001). Fault *f9* have a dip in the SE direction. The source locations of fault (*f9*) ranged from 231 to 603 m.

The magnetic profile F-F' was taken in the NW-SE direction in the northwestern part of the study area and covers a distance of 21.6 km. This profile (Figure 18) was modelled as ten (10) basement blocks. The observed magnetic intensity along the profile ranged from -62.76 to 40.44 nT. The Euler depth solutions across the profile ranged from 120.3 to 655.8 m. Blocks 2 and 3 are displaced by a lineament labelled *f1*1 while block 7 is displaced by fault *f9*. The magnetic response from both faults is a typical representation of a dyke and this confirmed them as a fault. The depth locations of fault *f9* occur from 120 to 340 m. Block 9 also show the magnetic response of a dyke displaced by a minor fault along the profile as shown in Figs. 11 and 12.

The direction of profile G-G' was taken across faults *f6* and *f7* from SW to NE around Sengiakun in the northwestern of the study area. This profile covers a distance of 27.5 km as shown in Figure 19. The intensity of the magnetic anomalies ranged from -85.57 to 37.76 nT. Judging by the presence of the V-shaped anomalies above blocks 5 and 8 which are displaced by faults *f6* and *f7* respectively, it is mostly likely a thin dyke. These confirmed the faults earlier explained on profile D-D'. The susceptibilities of blocks 5 and 8 is 0.002 and 0.003 cgs respectively which is relatively high than the surrounding blocks. The depth of occurrence of faults *f6* and *f7* ranged from 191to 655 m and 368 to 547 respectively.

The direction of profile H-H' was taken across faults *f4* from NE to SW around Kaya in the northeastern of the study area. This profile covers a distance of 26.3 km as shown in Figure 20 and was modelled as twelve (12) blocks. The intensity of the magnetic anomalies ranged from -52.55 to 25.32 nT while the susceptibility of the modelled blocks ranged between 0.001 to 0.002 cgs. Blocks 4 to 7 are displaced by a major fault *f4* which shows a magnetic response of a thick dyke as earlier shown on profile C-C'. Profile C-C' and H-H' both confirmed that fault *f4* is a fault zone dipping NE. Block 11 is displaced by fault *f1*0 and has vertical dip.

The magnetic profile I-I' was taken in the NW-SE direction in the northwestern part of the study area across fault *f2* and covers a distance of 22.8 km as shown in Figure 21. Block 6 is displaced by fault *f2*. The magnetic response above block 6 shows that fault *f2* is a thick dyke. This has been shown with profile A-A' and B-B'. However, profile A-A', B-B' and I-I' confirmed the Zungeru-Kalangai fault (*f2*) as a fault zone and also dipping SE. The observed magnetic intensity along the profile ranged from -73.87 to 24.76 nT.

Profile J-J' was taken across the upper part of fault *f3* around Malan Mudi in the northern part of the study area. This profile covers a distance of 23.5 km as shown as shown in Figure 22. The observed magnetic intensity along the profile ranged from -216.0 to 46.23 nT. Profile J-J' was modelled as four (4) blocks with susceptibility ranging from 0.001 to 0.006 cgs. Block 3 is displaced by fault *f3* whose susceptibility is higher (0.006 cgs) than the surrounding blocks (0.001 cgs). The shape of the anomaly above block 3 and its high susceptibility indicate it is likely a thin dyke (intrusion).

The possible 2D models of the basement blocks along the selected profiles shows and confirm the faults, their approximate source locations and dips (Figs. 13 - 22). The results of these models are in agreement with the results of the application of THD, ASA and ED methods to the HRAD. The results confirmed the existence of the Zungeru-Kalangai fault zone and other several hitherto undetected faults such as faults *f3* (northern part of the study area), *f4* (located around Kaya in the northeastern part of the study area), *f6* and *f9* (located around Sengiakun area in the northwestern part of the study area). The structural attributes of some of the inferred faults delineated are shown on Table 1.

6. Summary and Conclusion

Integrated satellite imagery (Landsat-7 ETM+) and High Resolution Aeromagnetic Data (HRAD) have been employed to confirm the existence of the Zungeru-Kalangai fault zone in Nigeria. In order to delineate the possible contact locations, depths, strikes, dip directions of faults and their surface expression within the study area, the geologic lineaments from remotely sensed data and magnetic lineaments from the aeromagnetic data were analysed and used to produce 2D models of the subsurface structures. The lineaments trend on the Landsat ETM+ showed a prominent lineament trend in N-S, NE-SW and NNE-SSW directions. The lineaments trending in the NE-SW direction are dense around Zungeru, Tegina and Gidan Karauku area enclosing the mylonites that might have been produced as a result of Pan-African shearing. The identified structural trends on the HRAD strike N-S, NNE-SSW, NW-SE, ENE-WSW, E-W, NE-SW, WNW-ESE and. The orientation (NE-SW) and location of the inferred fault emanating from the Bogi-Zungeru area (southwestern) to the Giwa area (northeastern) on the magnetic lineament map suggest a significant fault in the study area. This major fault was bisected by a NW-SE fault, thereby creating a conjugate pair on the fault at Kaya area (northeastern part).

Comparing the lineaments extracted from the HRAD and satellite imageries with the existing faults digitized from the geological map of Nigeria showed significant correlation between the location and orientation of the Zungeru-Kalangai fault zone in the northern part of Nigeria. Many other NE-SW trending faults within the study area could be associated with the stress history of Zungeru/Kalangai fracture system. Close lineaments in the same orientation/direction with the Zungeru/Kalangai fault show they are likely to have the same tectonic origin. The fracturing might have resulted as a response to the regional stress propagating through the study area in approximately NE-SW direction. The surface lineaments are denser on the Landsat ETM+ imagery than on the HRAD due to the fact that the datasets respond to different physical properties (surface radiation reflectance and susceptibility

contrast of rocks) of the geological units. Ten profiles were selected across the anomalies reflecting prominent structures and modelled to reveal the 2D image of the basement fault blocks and their depths. The variations in magnetic susceptibility of the basement rocks was revealed and low magnetic susceptibilities of rocks observed on the models were due to the fractured bedrock within the study area. These were used to confirm geophysically the existence of the Zungeru-Kalangai fault zone which is dipping SE and other mapped major structures in the study area.

This study concluded that the Zungeru-Kalangai fault zone do exist and that the fault zone dip SE with a conjugate fault pair around Kaya area. It was observed that the fault zone possibly propagated into the study area through the Bida Basin. The regional field stress associated with the Zungeru-Kalangai fault zone would have played an essential role on the faulting system of the area. The presence of several major lineaments with and without surface expression corresponding to some unknown and known faults were revealed with the combined interpretation of satellite imageries and HRAD.

Acknowledgements

The aeromagnetic data that support the findings of this study are property of Nigerian Geological Survey Agency (NGSA) and are available on request to A.B. Arogundade while the satellite imagery (Landsat ETM+) data are available and can be freely downloaded, after registration, at the following URL: http://glovis.usgs.gov.

References

Adepelumi, A. A. Ako, B. D., Ajayi, T. R., Olorunfemi, A. O., Awoyemi, M.O., and Falebita, D.E (2008). Integrated geophysical mapping of the Ifewara transcurrent fault system, Nigeria, Journal of African Earth Sciences, 52, 161-166.

Ajakaiye, D. E., Hall, D. H., Millar, T. W., Verheijen, P. J. T., Aurad, M. B. and Ojo, S. B. (1986). Aeromagnetic anomalies and tectonic trends in and around the Benue Trough, Nigeria. Nature, 319, 582-584.

Ajibade, A. C., Fitches, W. R., Wright, J. B. (1979). The Zungeru mylonites, Nigeria: recognition of a major unit. Rev de Geol Geog Phys 21:359–363.

Awoyemi M. O., Hammed O. S., Falade S. C., Arogundade A. B., Ajama O. D., Iwalehin P. O., Olurin O. T. (2017a). Geophysical investigation of the possible extension of Ifewara fault zone beyond Ilesa area, southwestern Nigeria. Arabian Journal of Geoscience, 10:27. 1-14.

Awoyemi M. O., Ajama O. D., Hammed O. S., Arogundade A. B., Falade S. C., (2017b). Geophysical mapping of buried faults in parts of Bida Basin, North Central Nigeria. Geophysical Prospecting, 66, 40–54.

Chavez, P. S., Berlin G. L. and Sowers L. B., (1982). Statistical method for selecting Landsat MSS ratios. Journal of Applied Photographic Engineering, 8: 23-30.

Gettings M.E. (2005). Multifractal magnetic susceptibitlity distribution models of hydrothermally altered rocks in the needle creek igneous center of the Absaroka Mountains, Wyoming. Nonlinear Processes in Geophysics, 12, 587-601.

Grant, N. K. (1978). Structural distinction between a metasedimentary cover and an underlying basement in the 600 my old Pan-African domain of Northwestern Nigeria. Geol Soc Am Bull 89:50–58.

Hung, L. Q., Batelaan O., and De Smedt F. (2005). Lineament extraction and analysis, comparison of LANDSAT ETM and ASTER imagery. Case study: Suoimuoi tropical karst catchment, Vietnam. Edited by Manfred Ehlers, Ulrich Michel, Proc. of SPIE. 5983, 1-12.

Isaksson, H., Thunehed, H., Pitkänen, T. and Keisu, M. (2007). Forsmark site investigation: Detailed ground magnetic survey and lineament interpretation in the Forsmark area, 2006-2007. Swedish Nuclear Fuel Management AB, SKB R-07-62

Kolawole, F. and Anifowose, A. Y. B. (2011). Remote sensing analysis of a dextral discontinuity along Ifewara-Zungeru area, Nigeria, West Africa. Indian Journal of Science and Technology. 4 (1), 46-51.

Mallast, U., Gloaguen, R., Geyer, S., Rodiger, T. and Siebert, C. (2011). Derivation of groundwater flow-paths based on semi-automatic extraction of lineaments from remote sensing data. Hydrol. Earth Syst. Sci. Disc., 5, 2665–2678.

McCurry, P. (1971). Pan-African Orogeny in Northern Nigeria. Geol. Sot. Am. Bull., 82: 3251-3262.

McCurry, P. (1976). The geology of the Precambrian to Lower Palaeozoic Rocks of Northern Nigeria – A Review. In: Kogbe CA (ed) Geology of Nigeria. Elizabethan Publishers, Lagos, 15–39.

Nigeria Geological Survey Agency (NGSA) (2004). Geological Map of Nigeria (2004 Ed.).

Obaje, N.G. (2009). Geology and Mineral Resources of Nigeria, Lecture Notes in Earth Sciences 120. Springer-Verlag, Berlin.

Olade, M.A.and Elueze, A.A. (1979). Petrochemistry of the Ilesha amphibolite and Precambrian crustal evolution in the Pan-African domain of SW Nigeria. Precambrian Res 8:303–318

Olasehinde, P. I., Pal, P. C., Annor, A. E. (1990). Aeromagnetic anomalies and structural lineament in the Nigerian Basement Complex. J Afr Earth Sci 11(3/4):351–355.

Oluyide, P. O. (1988). Structural trends in the Nigerian basement complex. In: Oluyide P.O., Mbonu W.C., Ogezi A.E., Egbuniwe I.G., Ajibade A.C., Umeji A.C. (eds.) Precambrian Geology of Nigeria, Geological Survey of Nigeria, Kaduna: 93-98.

Reid, A. B., Allsop, J. M., Granser, H., Millett, A. J. and Somerton, I. W. (1990). Magnetic interpretation in three dimensions using Euler deconvolution. Geophysics, 55, 80–90.

Turner, D. C. (1983). Upper Proterozoic schist belts in the Nigerian sector of the Pan-African province of West Africa. Precambrian Res. 21, 55-79.

Wright, J. B. (1976). Fracture systems in Nigeria and initiation of fracture zones in the South Atlantic. Tectonophvsics 34:43–47.

Wright, J. B. and McCurry, P. (1970). First occurrence of Manganese ores in Northern Nigeria. Econ Geol 65,103–106.

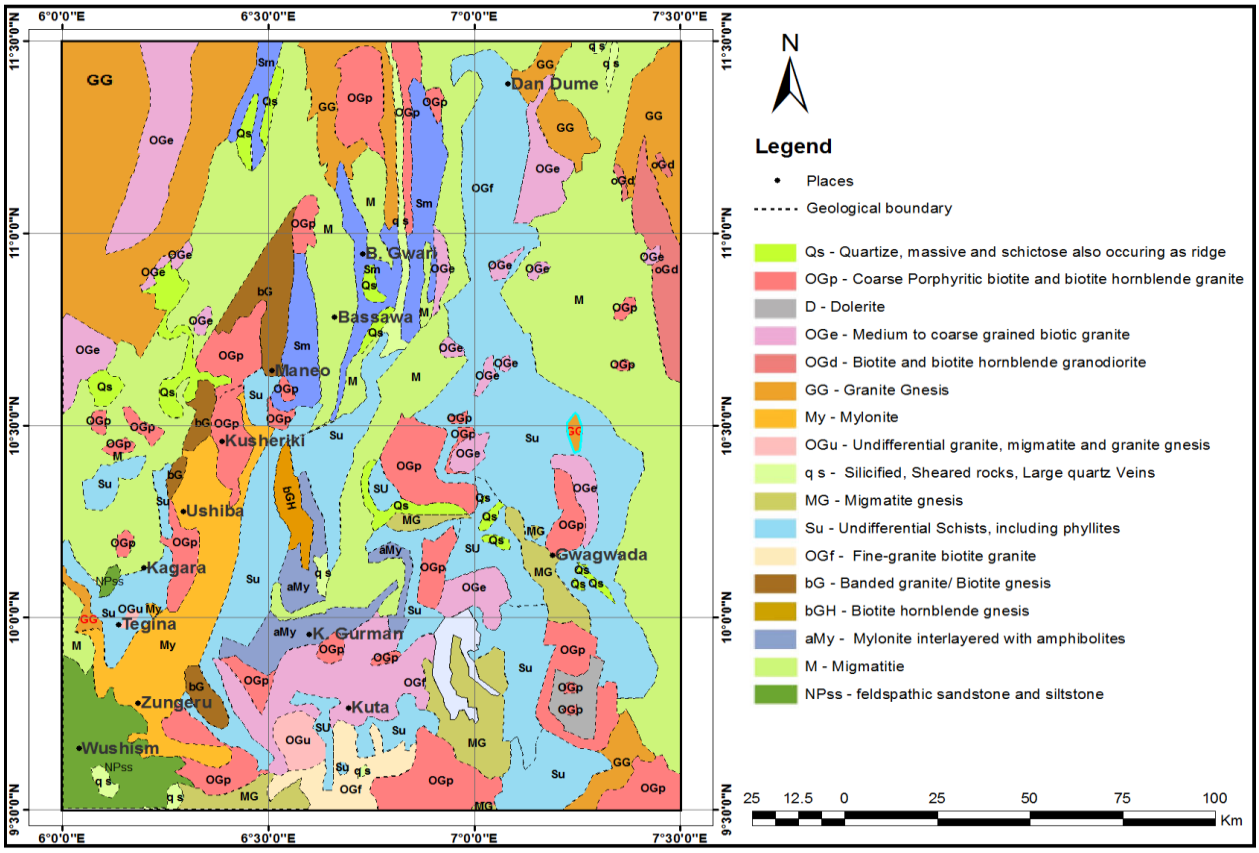

Figure 1: Geological map of the study area (Adapted from NGSA, 2004)

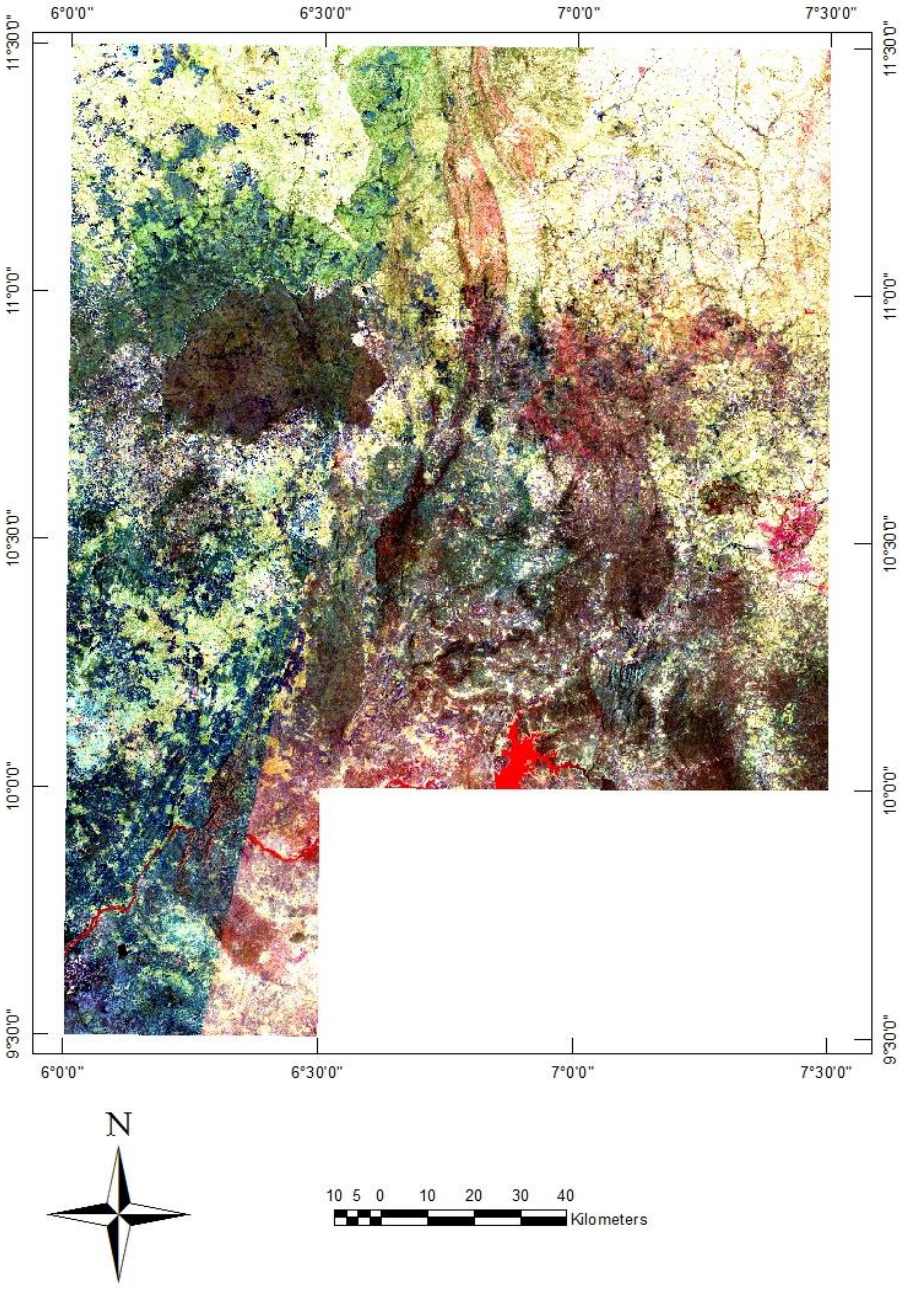

Figure 2: Landsat ETM+ false colour composite image (FCC) using bands 357 (RGB) suitably pan-sharpened, contrast stretched and edge enhanced

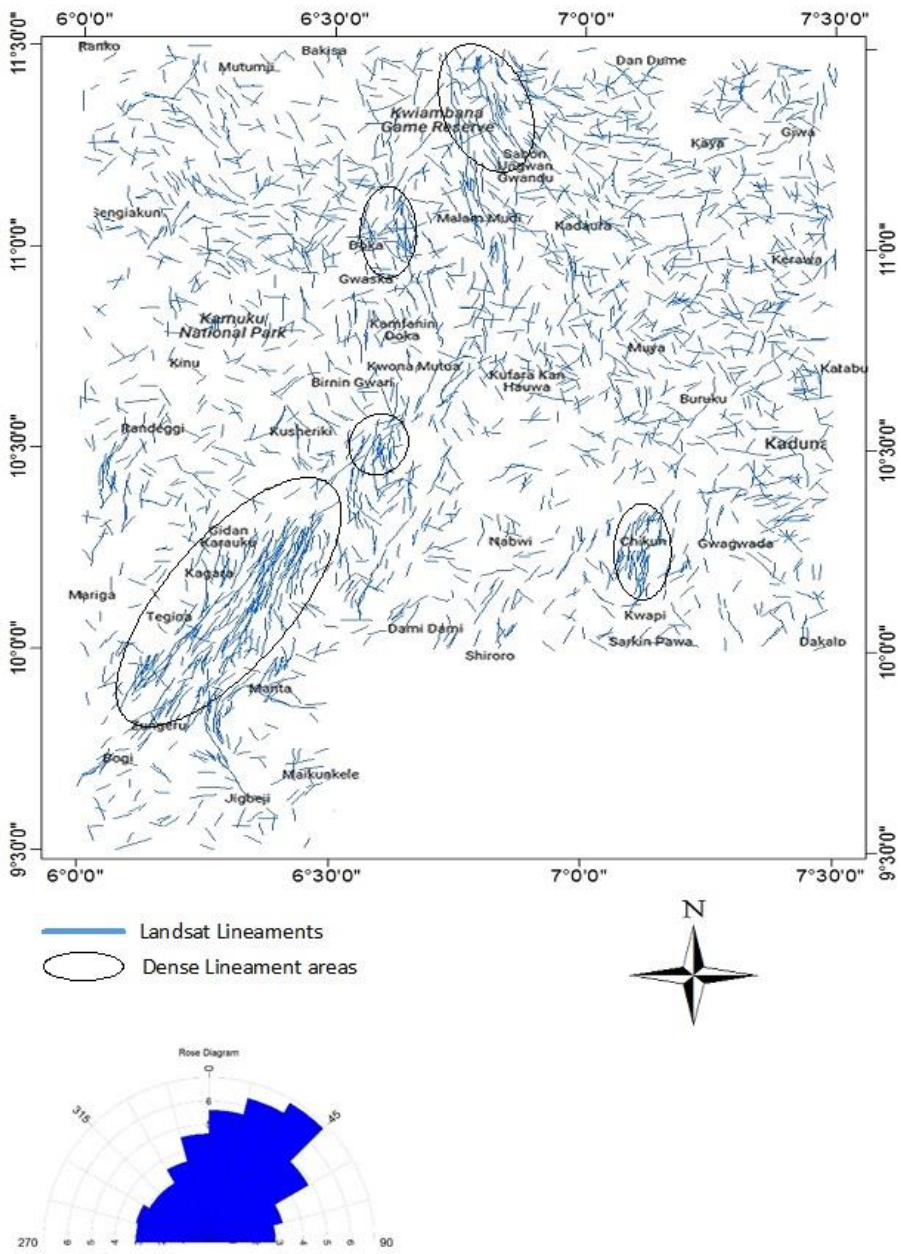

Figure 3: Landsat ETM+ lineament map of the study area

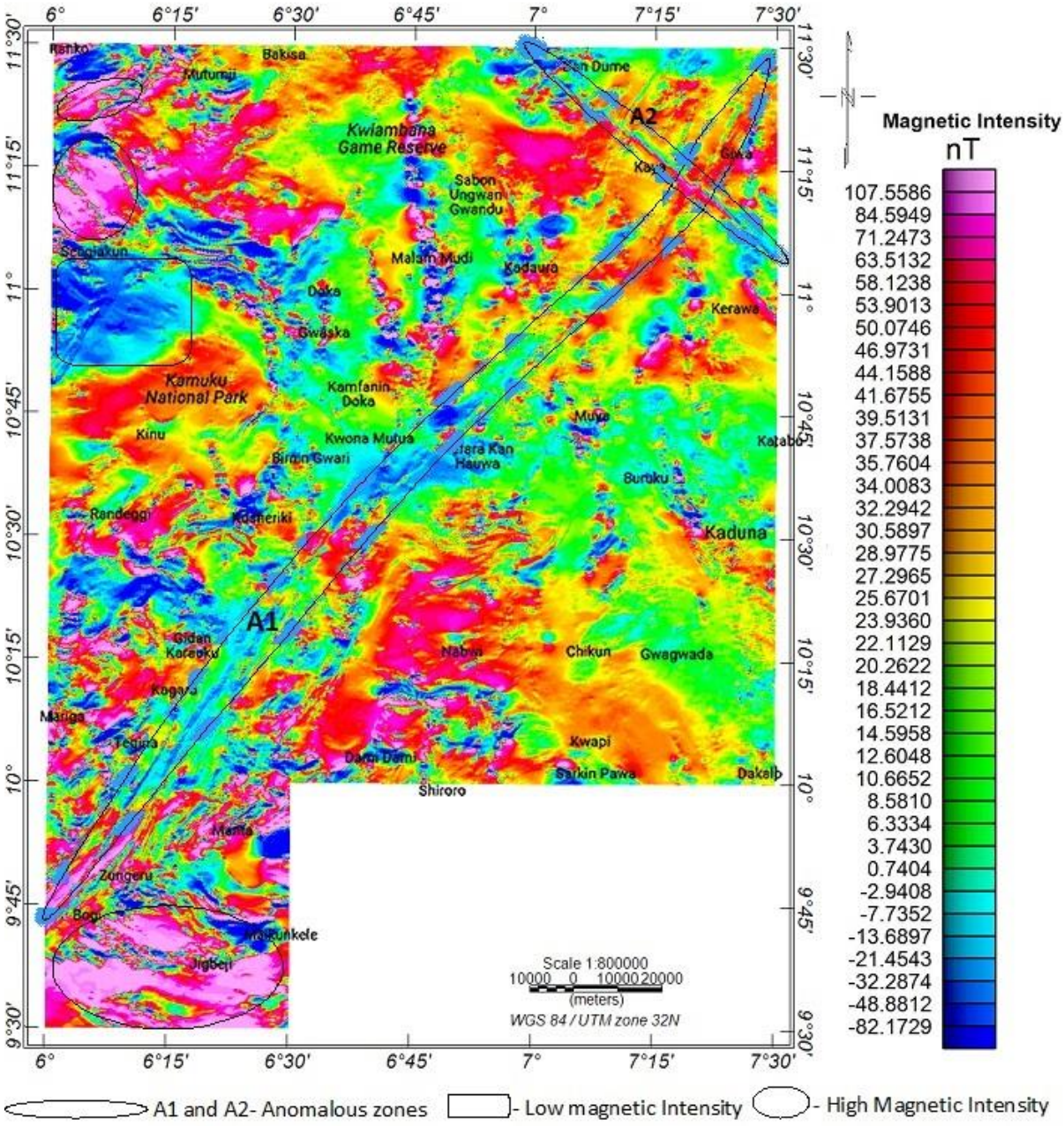

Figure 4: Total magnetic intensity (TMI) map of the study area

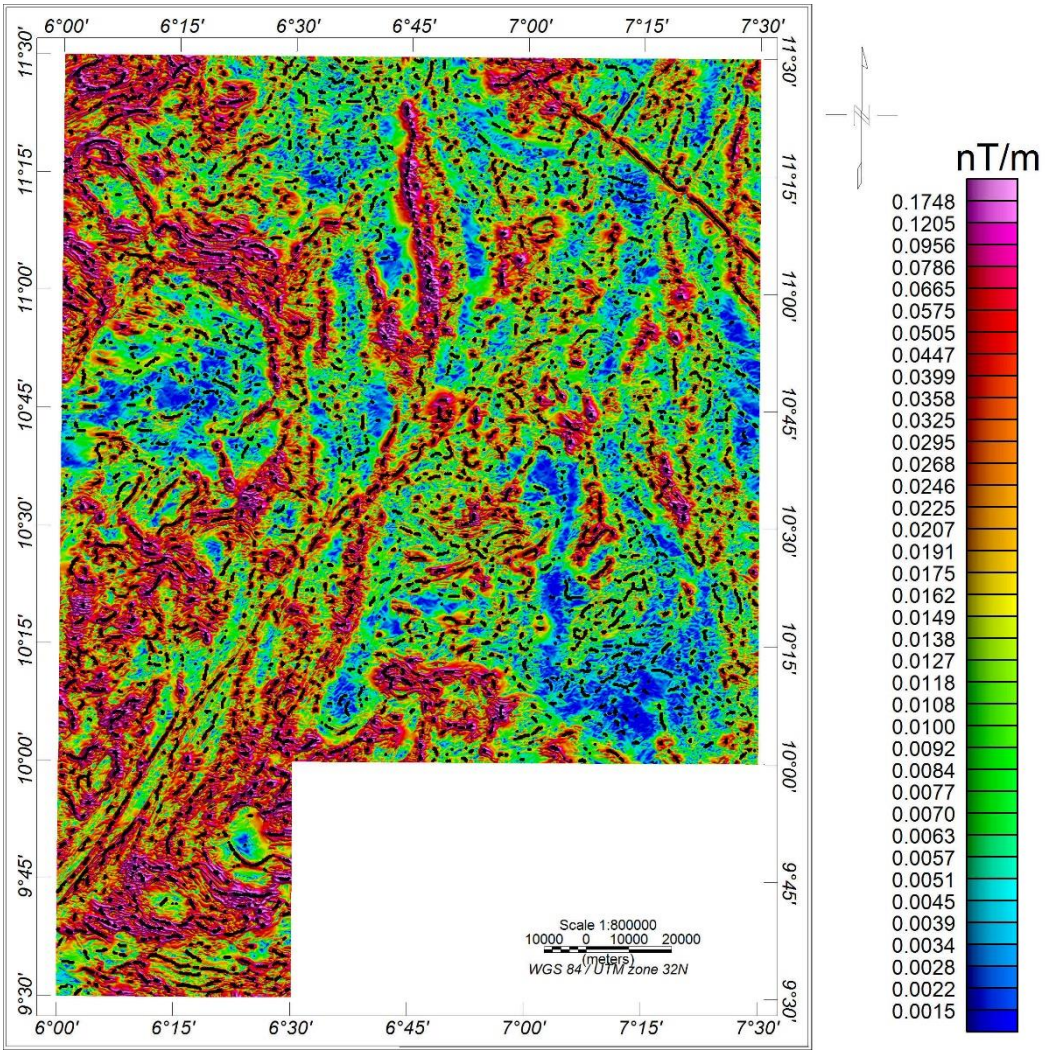

Figure 5: Total horizontal derivative map with maximum amplitude points overlain on the map

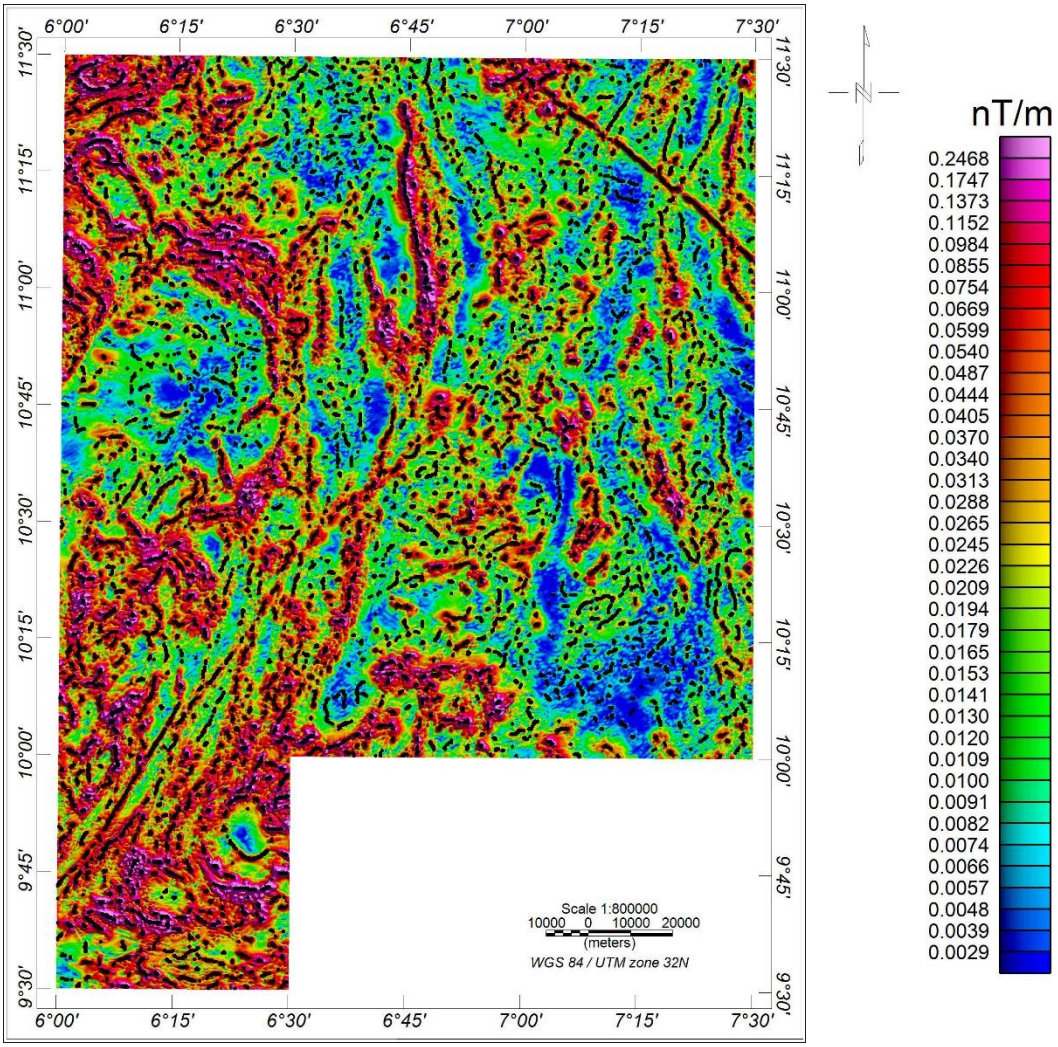

Figure 6: Analytic signal amplitude map with maximum amplitude points overlain on the map

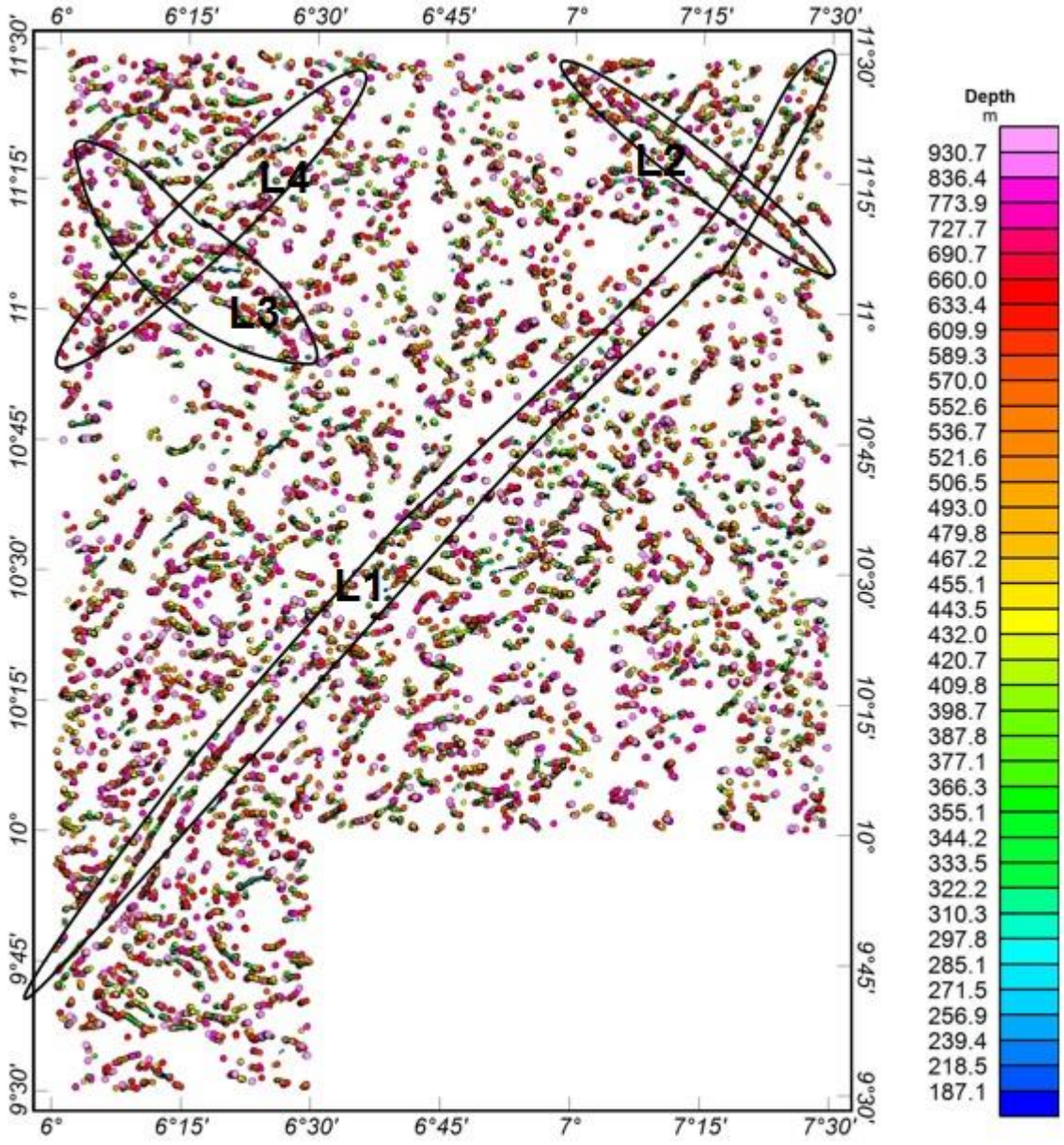

Figure 7: Euler solutions plot using structural index of 1 (depth varies with colour)

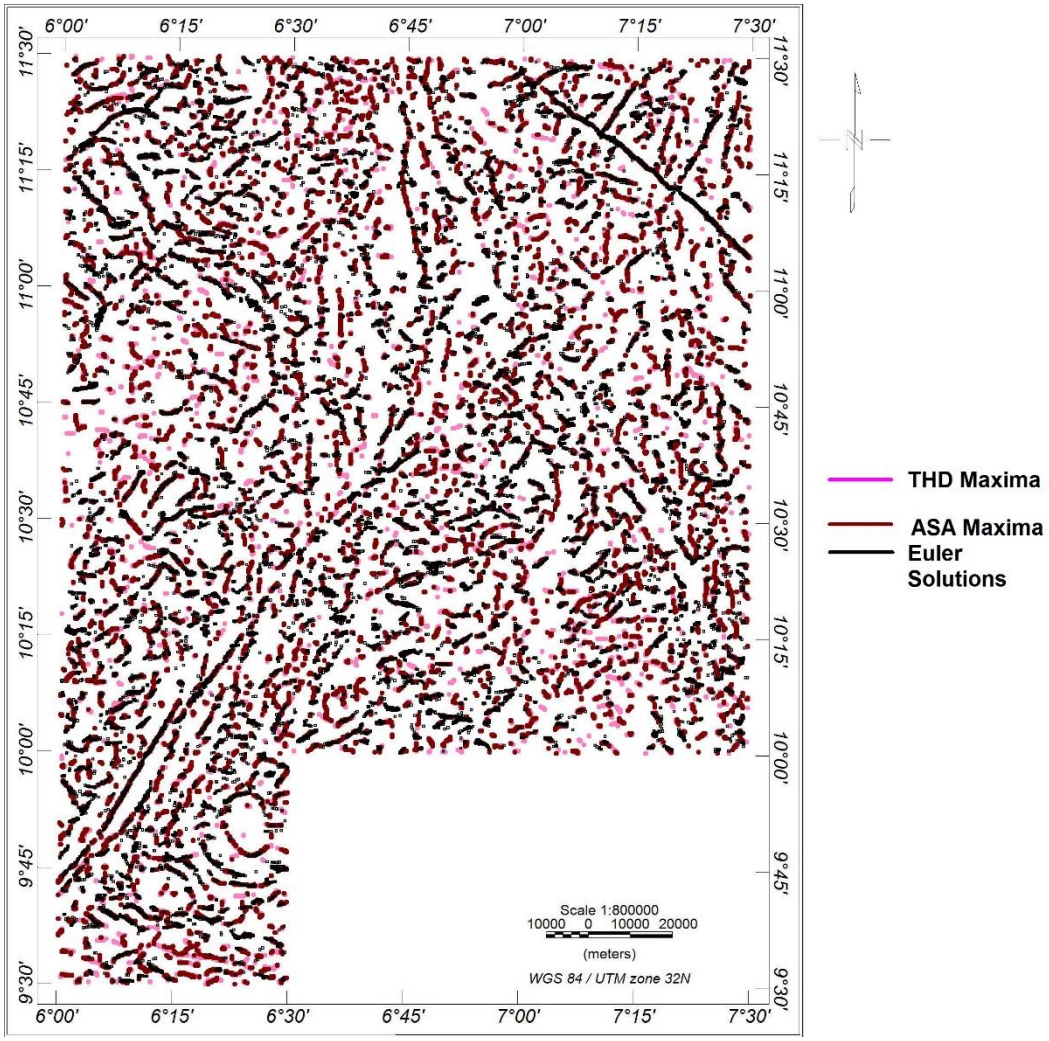

Figure 8: Composite Map of the estimated Locations from THD (pink), ASA (brown) and Euler Solutions (black)

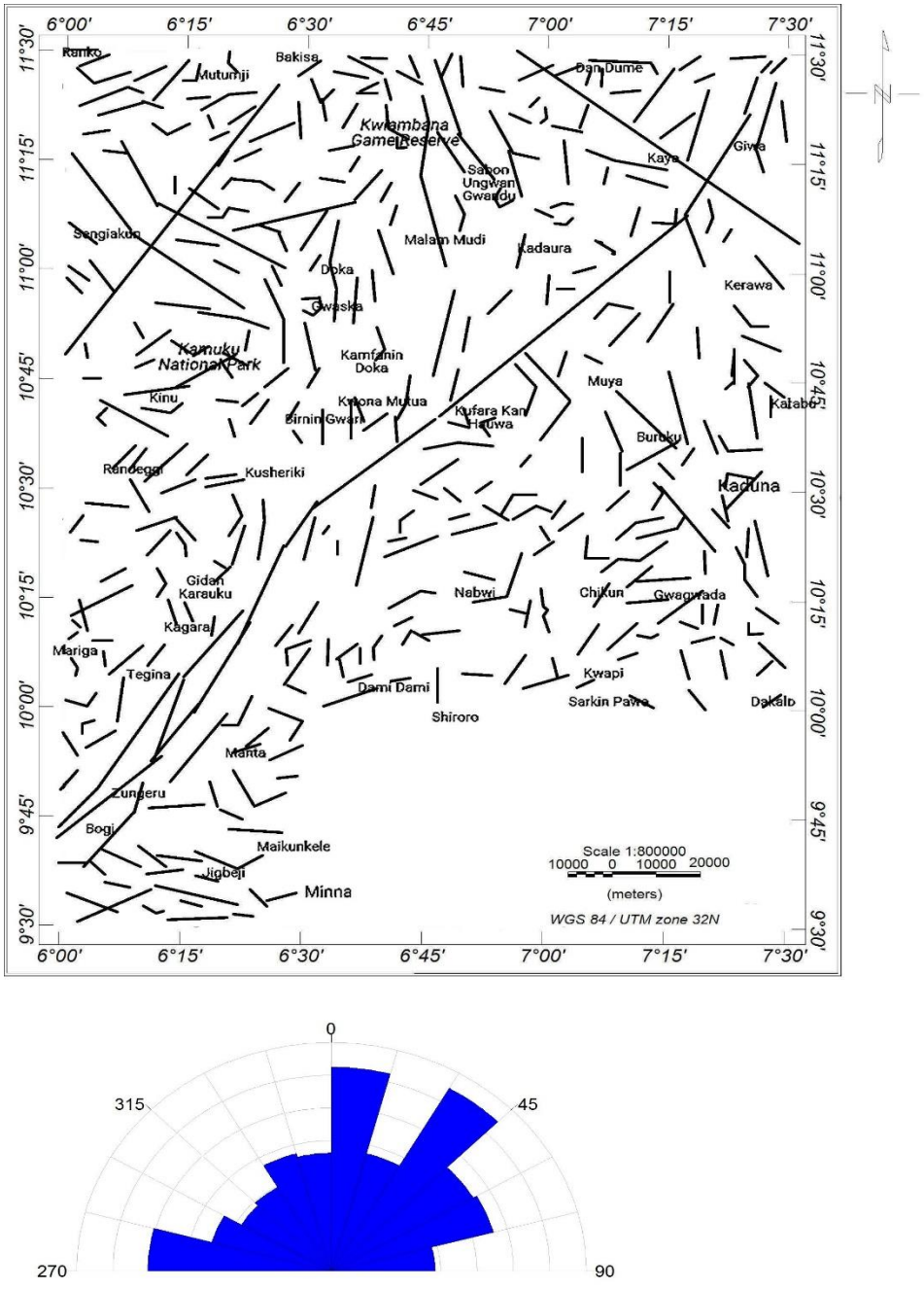

Figure 9: Inferred Contact Locations Map from THD and ASA

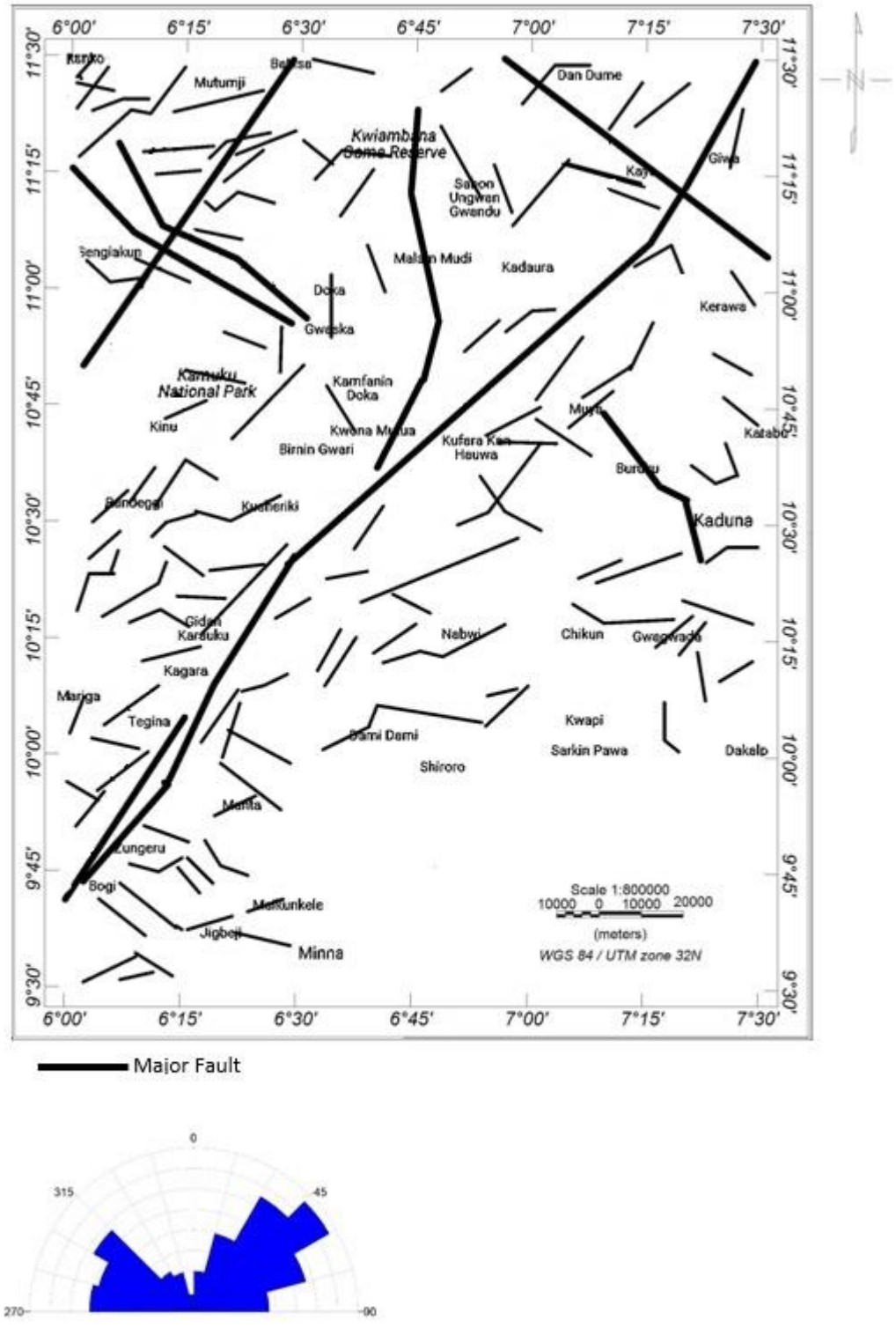

Figure 10: Lineament Map of the Study Area showing the Inferred Faults from the Composite Map of the THD, ASA and Euler Solutions

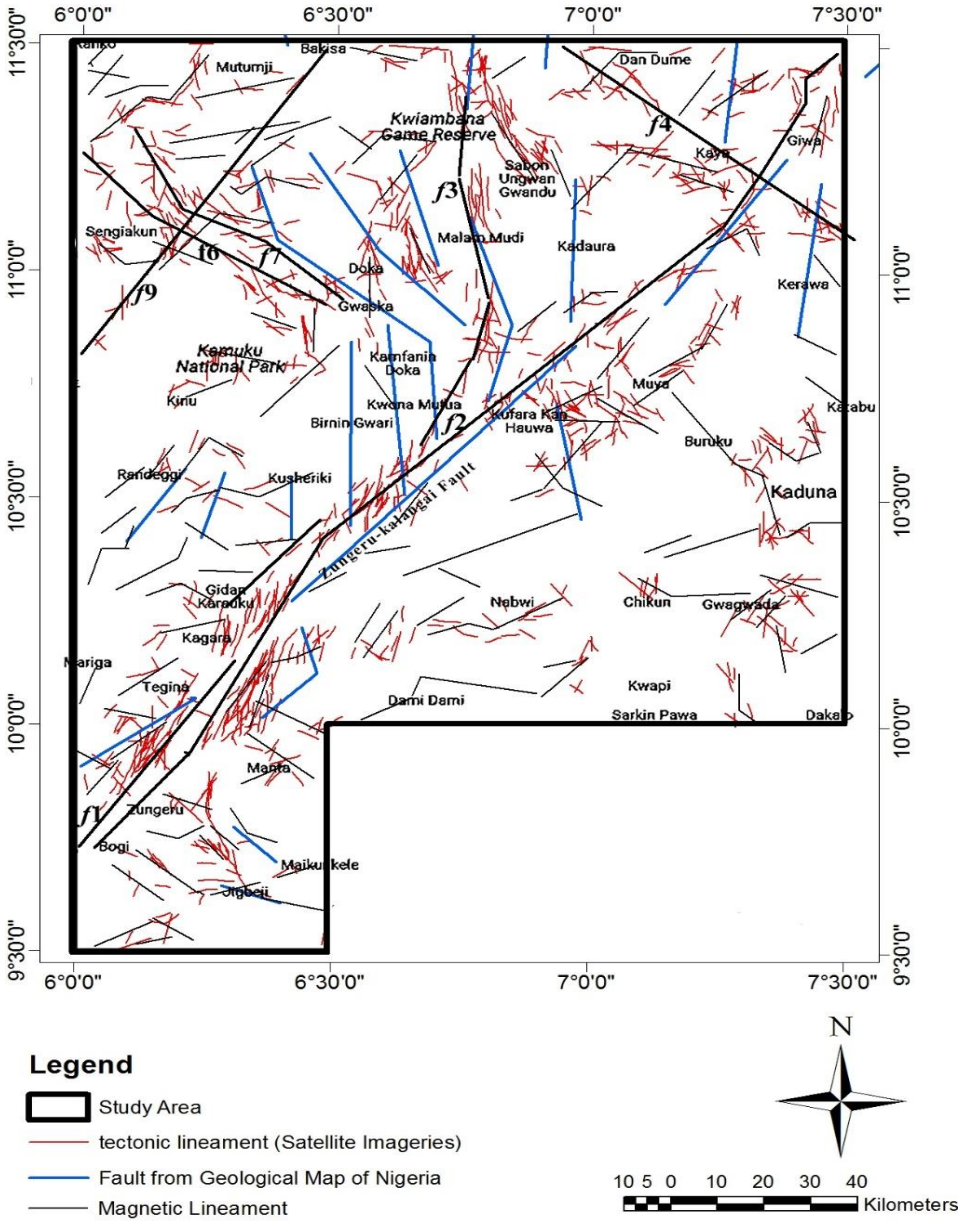

Figure 11: Composite lineament map of the inferred faults from HRAD and tectonic lineaments from the satellite imageries superimposed on the existing structural map of the study area.

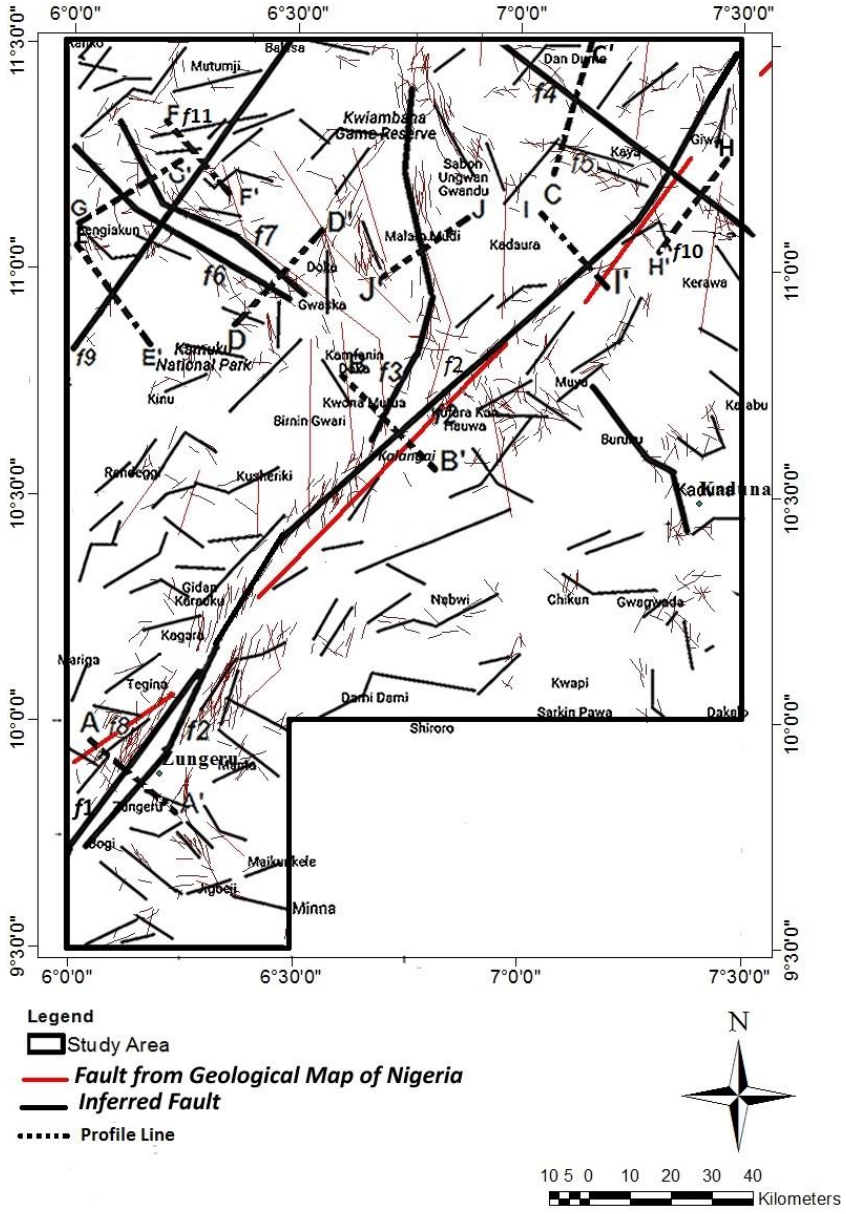

Figure 12a: Ten magnetic profiles drawn across major faults

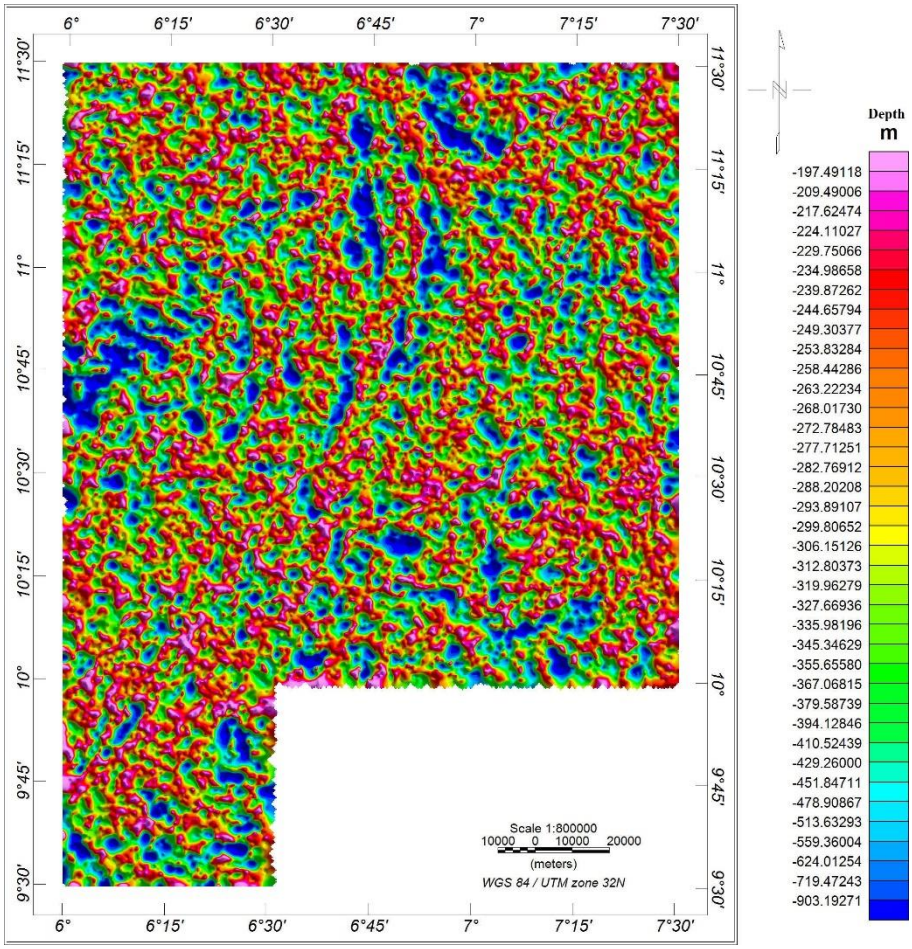

Figure 12b: SPI map showing variations in depth to across the study area

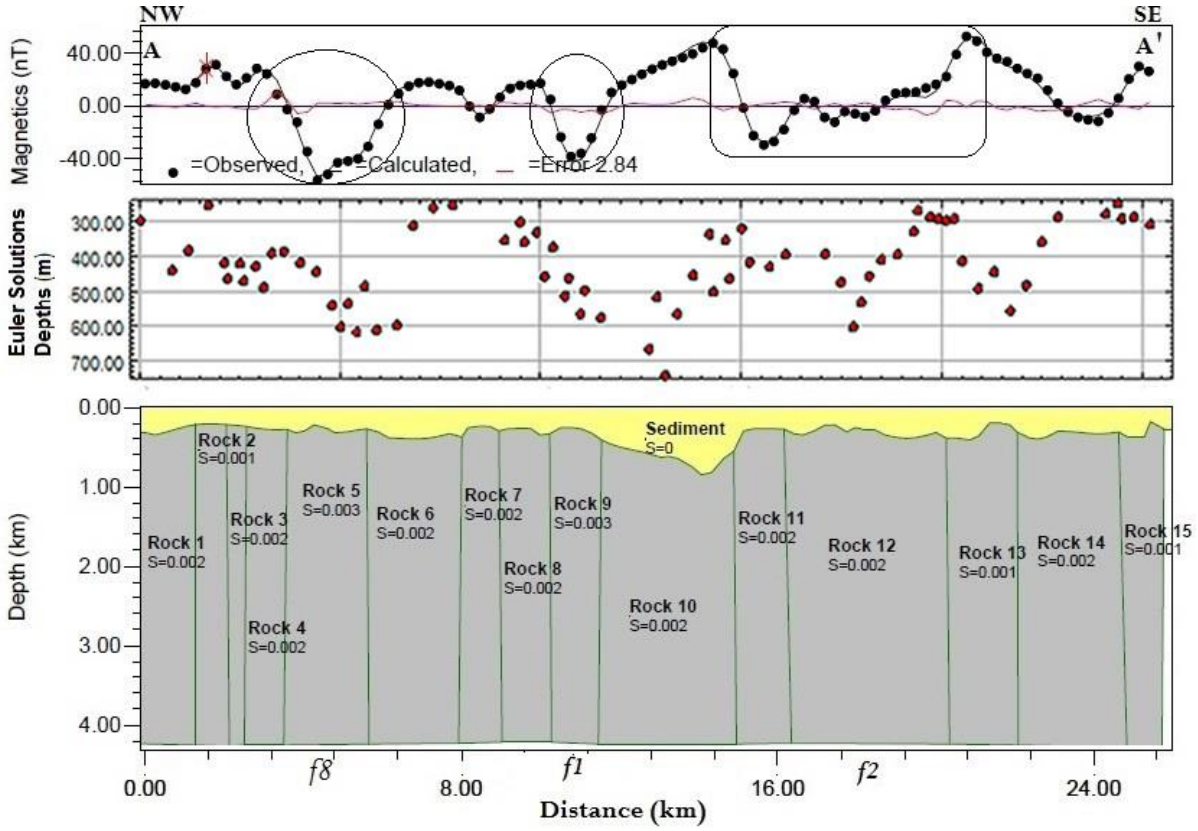

Figure 13: Geological model along profile A-A'

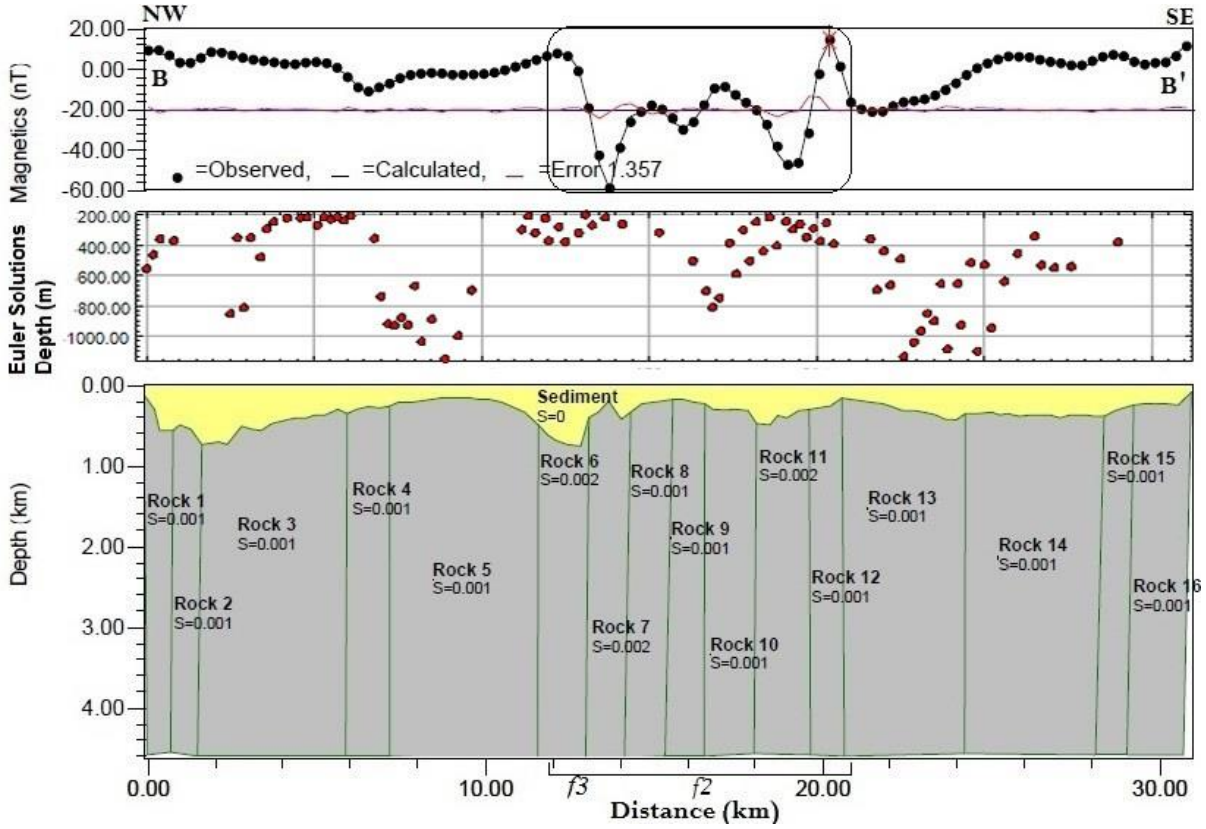

Figure 14: Geological model along profile B-B'

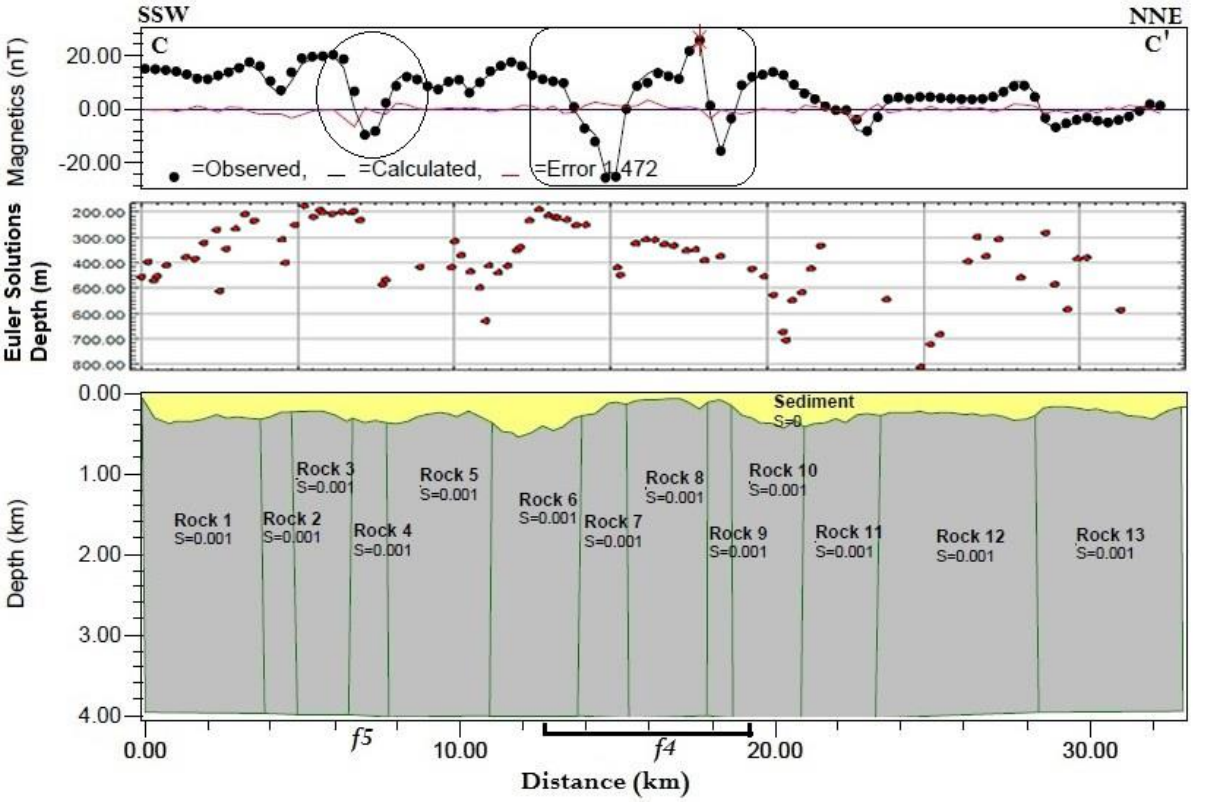

Figure 15: Geological model along profile C-C'

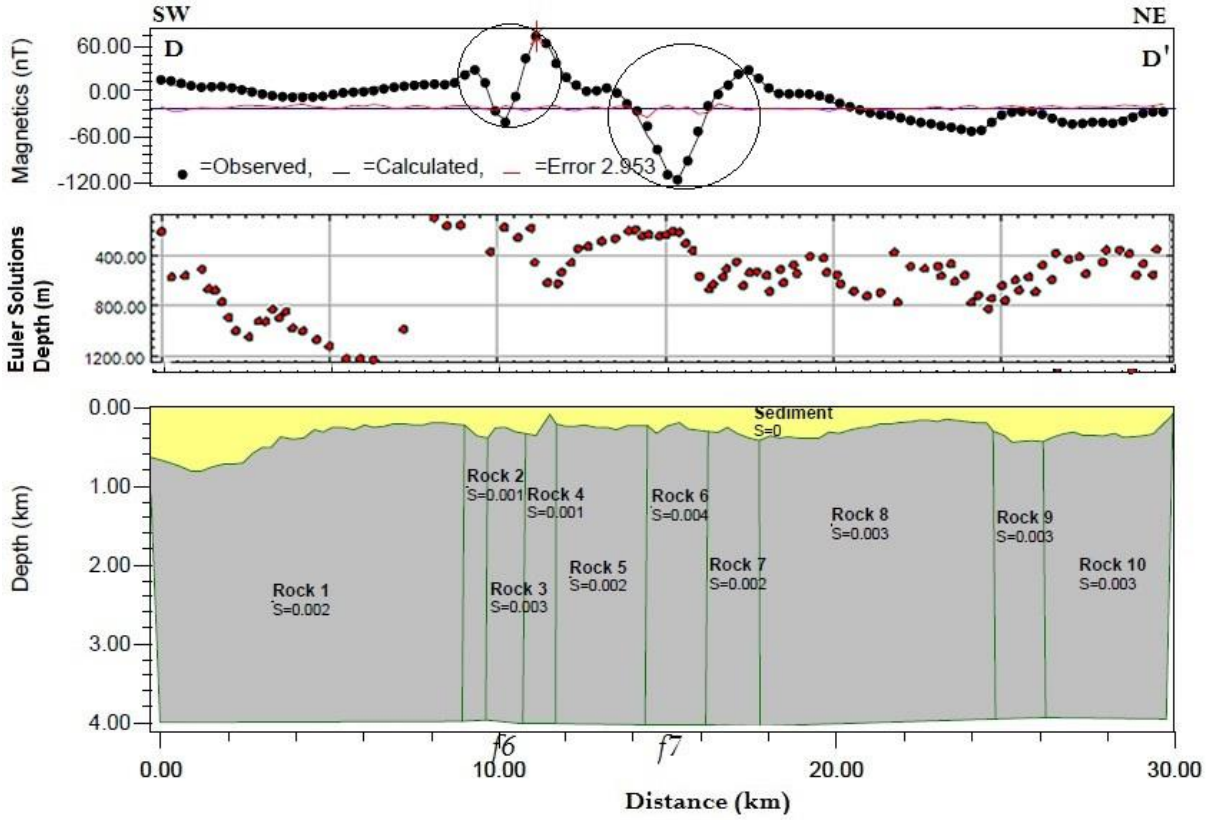

Figure 16: Geological model along profile D-D'

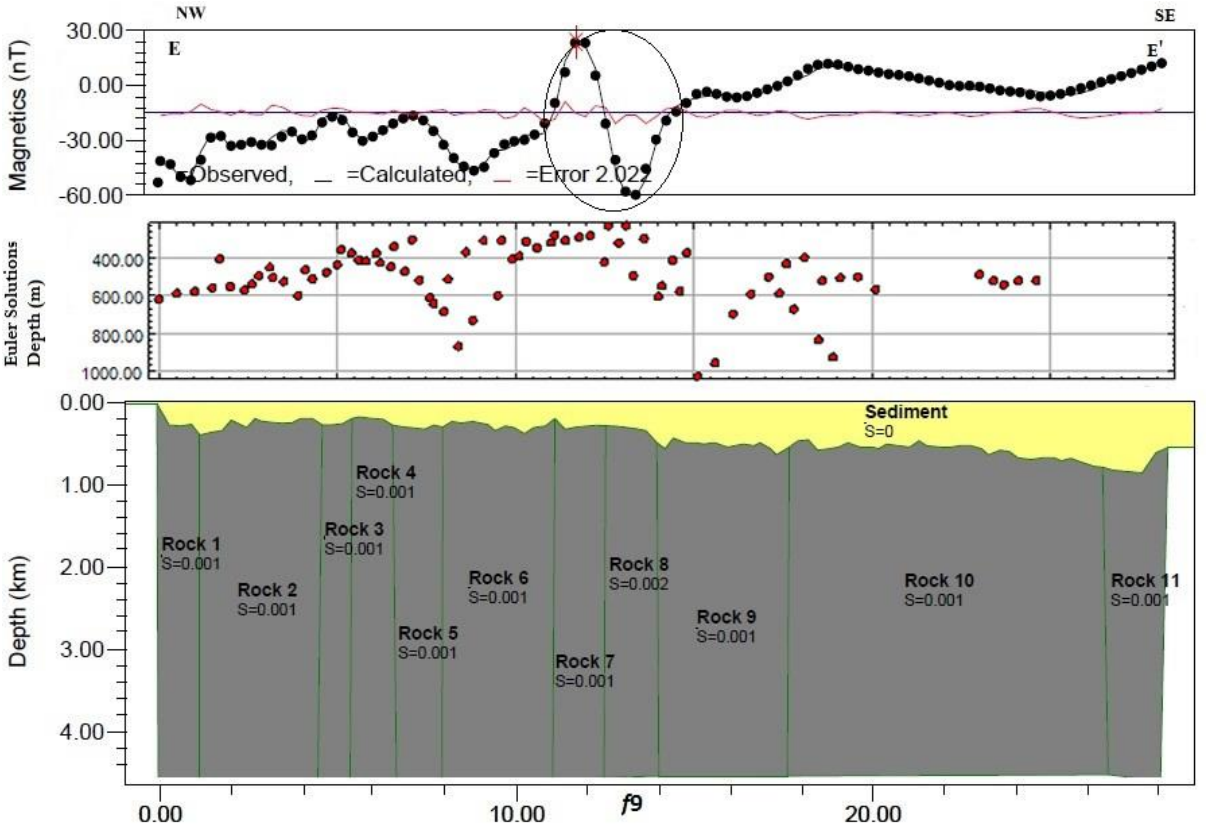

Figure 17: Geological model along profile E-E'

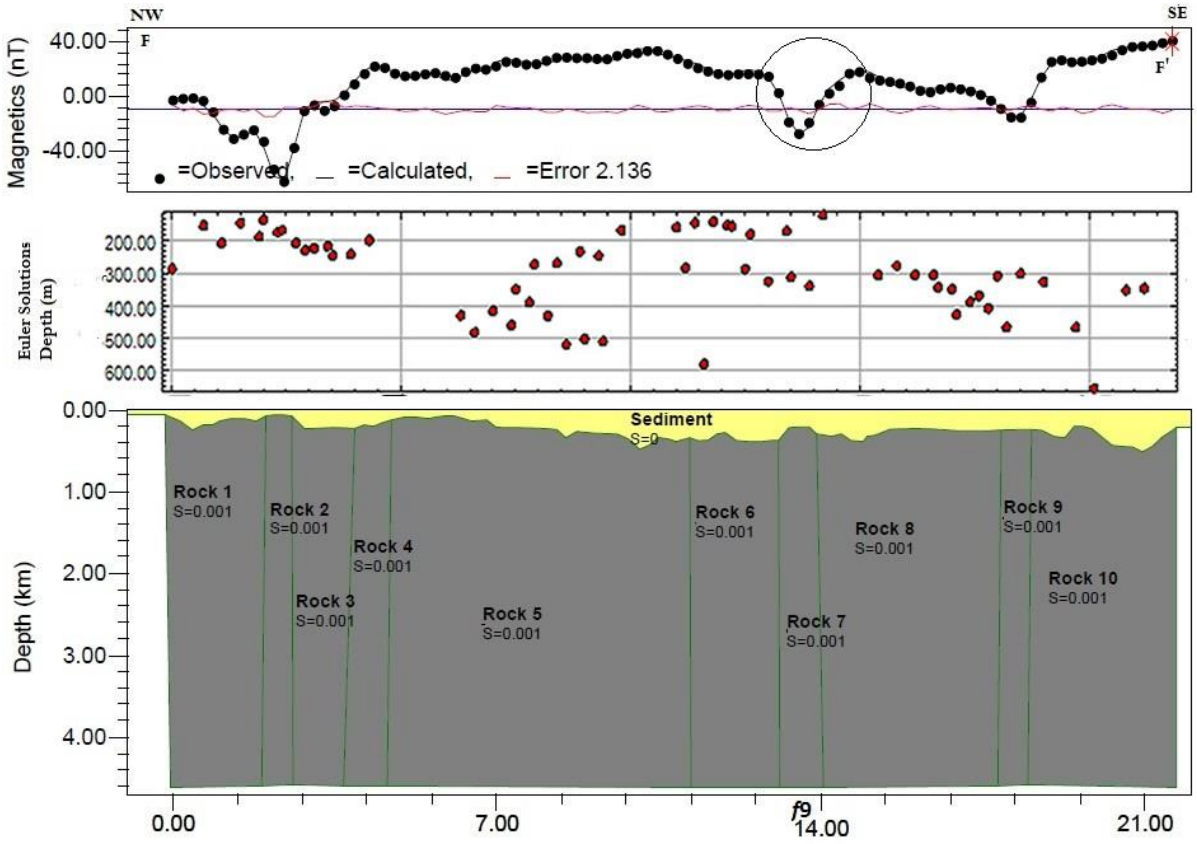

Figure 18: Geological model along profile F-F'

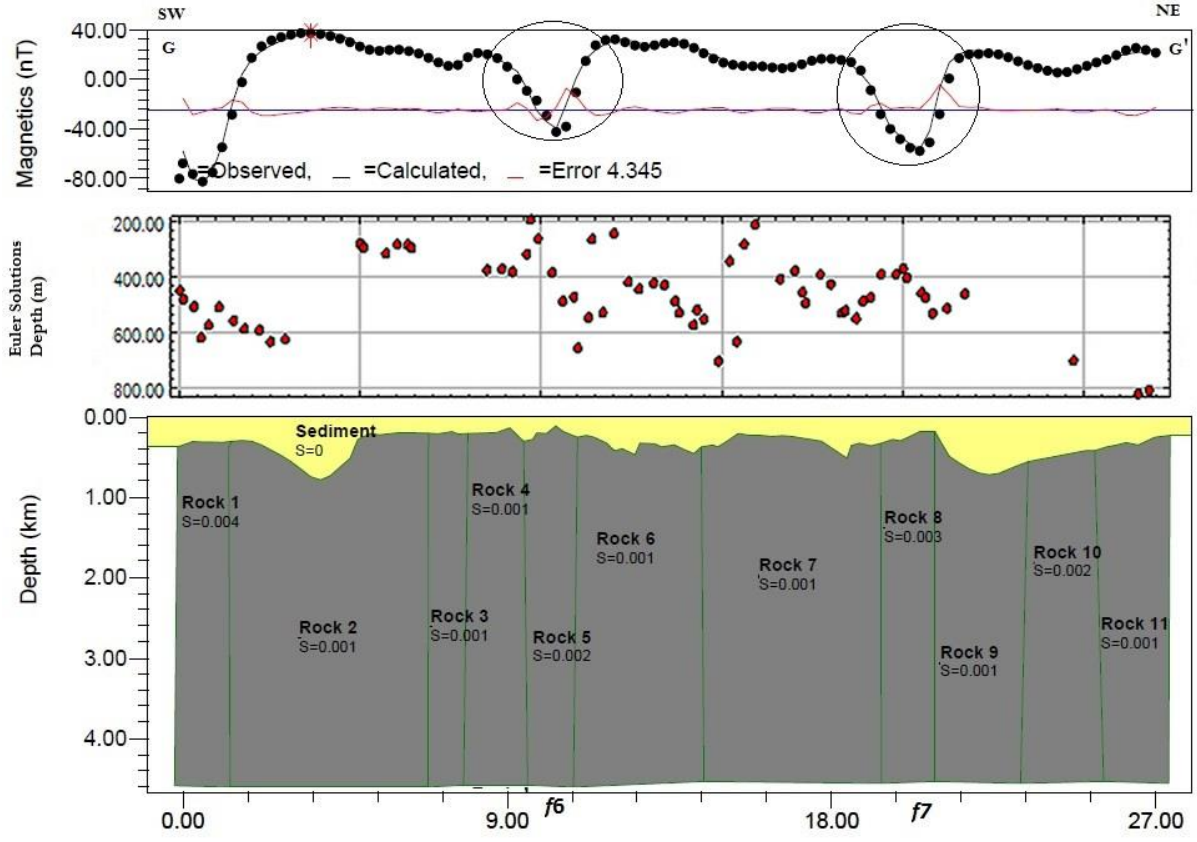

Figure 19: Geological model along profile G-G'

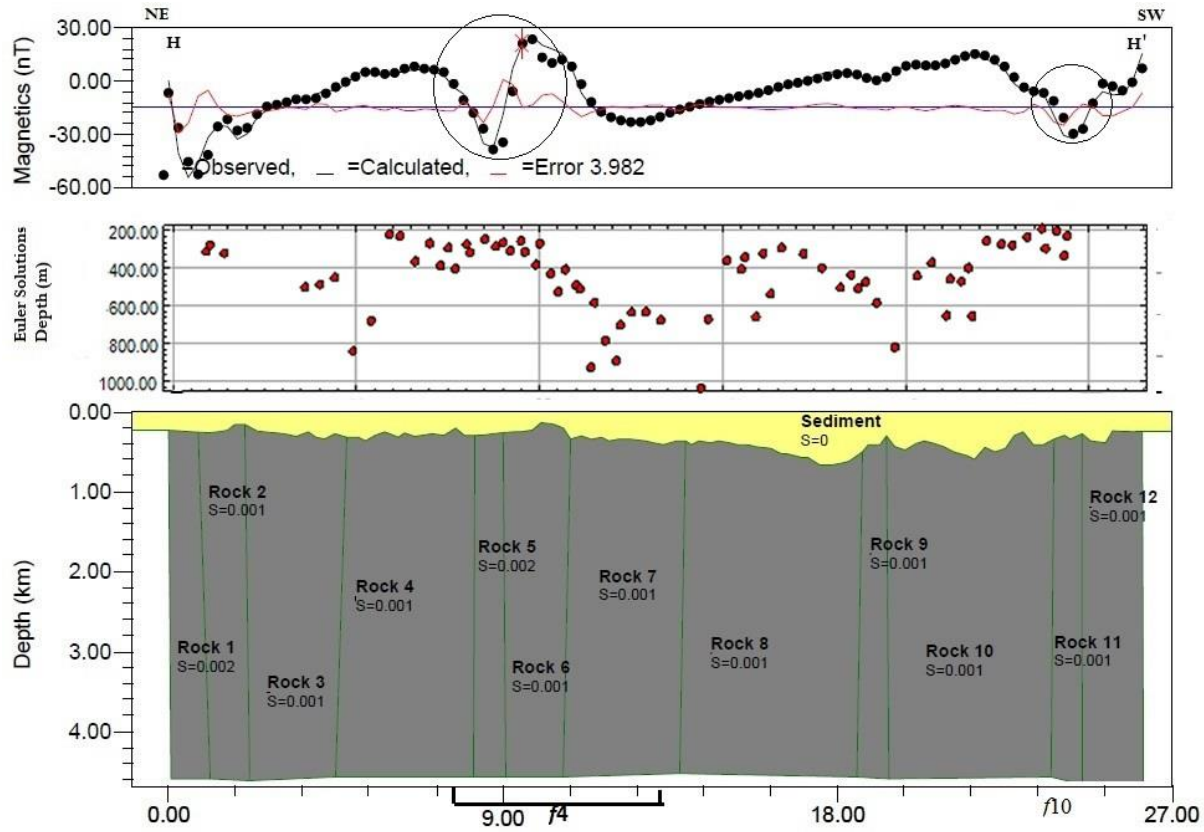

Figure 20: Geological model along profile H-H'

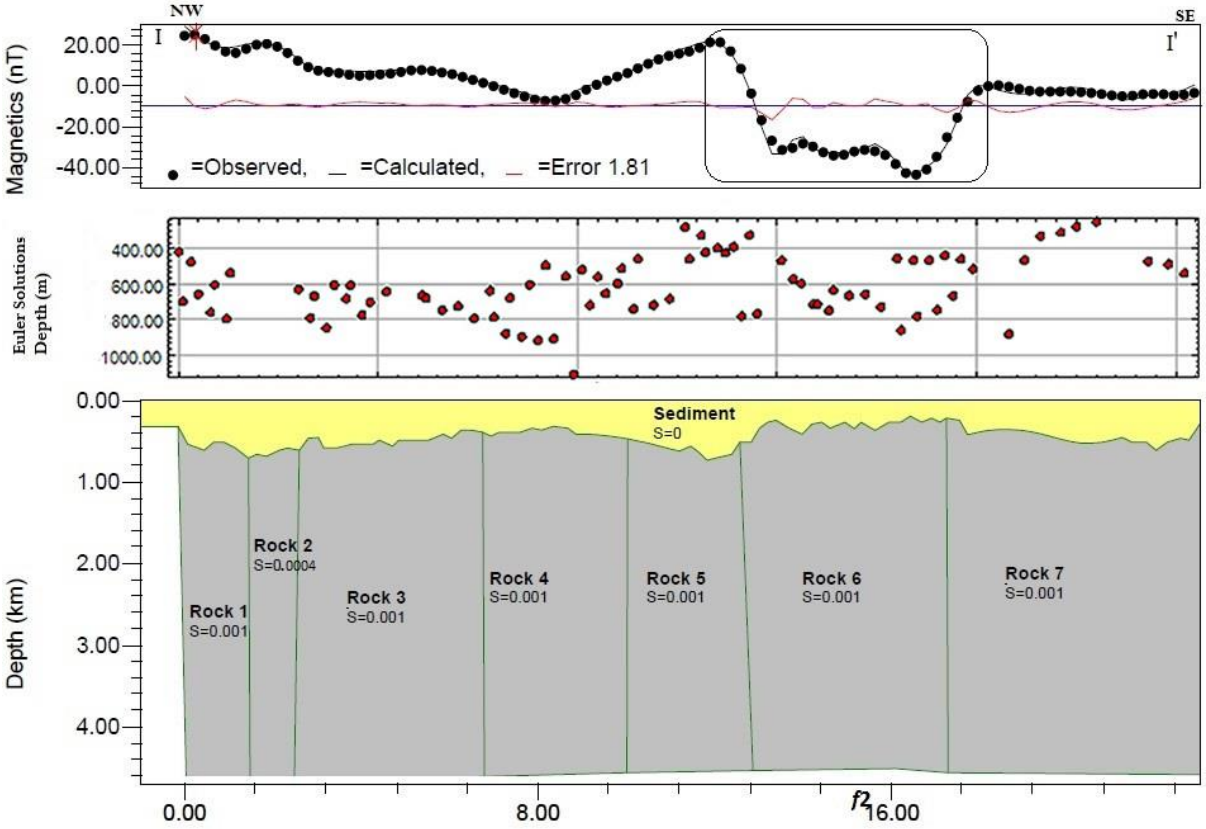

Figure 21: Geological model along profile I-I'

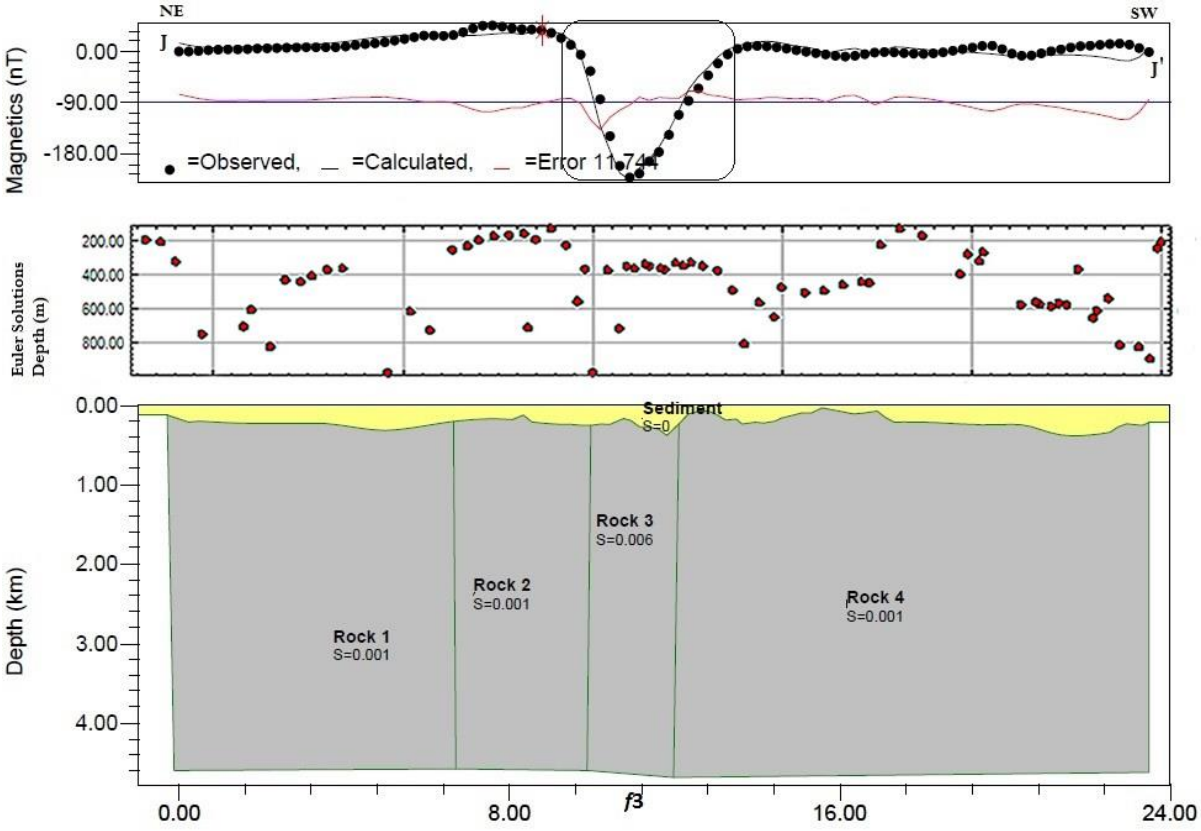

Figure 22: Geological model along profile J-J'